

Aus der Klinik für Strahlentherapie und Radioonkologie  
der Medizinischen Fakultät Mannheim  
(Direktor: Prof. Dr. med. Frederik Wenz)

**Development of a treatment planning algorithm for peptide-receptor  
radionuclide therapy considering multiple tumour lesions and  
organs at risk**

Inauguraldissertation  
zur Erlangung des Doctor scientiarum humanarum (Dr. sc. hum.)  
der  
Medizinischen Fakultät Mannheim  
der Ruprecht-Karls-Universität  
zu  
Heidelberg

vorgelegt von  
Luis David Jiménez Franco

aus  
Medellín, Kolumbien  
2018

Dekan: Herr Prof. Dr. med. Sergij Goerd

Referent: Herr Prof. Dr. med. Frederik Wenz

## TABLE OF CONTENTS

LIST OF FIGURES .....	iv
LIST OF TABLES .....	v
LIST OF ABBREVIATIONS .....	vi
1 INTRODUCTION.....	1
2 BACKGROUND .....	3
2.1 Molecular Radiotherapy.....	3
2.1.1 Radiopharmaceuticals in Molecular Radiotherapy .....	3
2.1.2 Peptide-Receptor Radionuclide Therapy .....	5
2.1.3 Radioimmunotherapy .....	6
2.2 Pharmacokinetics .....	8
2.3 PBPK Models .....	11
2.4 Dosimetry in Molecular Radiotherapy.....	14
2.4.1 Biologically Effective Dose .....	16
2.5 Treatment Planning in MRT.....	19
3 MATERIALS AND METHODS .....	23
3.1 Overall Biologically Effective Dose .....	23
3.2 Overall Tumour Control Probability.....	26
3.3 Virtual Patients .....	27
3.3.1 Patient Data .....	27
3.3.2 PBPK Model.....	28
3.4 Description of the Developed Treatment Planning Algorithm .....	29
3.5 <i>In Silico</i> Clinical Trial .....	35
3.6 Data Analyses and Statistics .....	36
4 RESULTS .....	37
5 DISCUSSION.....	43
6 CONCLUSIONS.....	47
7 SUMMARY .....	48
8 REFERENCES .....	50
APPENDIX A: Absorbed Dose Calculations .....	57
APPENDIX B: Liver and Spleen Results .....	60
CURRICULUM VITAE .....	61
PUBLICATIONS .....	62
ACKNOWLEDGEMENTS.....	63

## LIST OF FIGURES

<b>Figure 1.</b> Labelling techniques [24]. .....	4
<b>Figure 2.</b> Pretargeted radioimmunotherapy. ....	7
<b>Figure 3.</b> Time-activity curve and area under the curve.....	10
<b>Figure 4.</b> Two-compartment PBPK model.....	12
<b>Figure 5.</b> Whole-body PBPK model [4]. ....	13
<b>Figure 6.</b> Representation of the linear-quadratic model. ....	18
<b>Figure 7.</b> Algorithm for pharmacokinetic-model-based treatment planning in molecular radiotherapy (modified from Glatting et al. [7]).....	21
<b>Figure 8.</b> Workflow of the developed treatment planning algorithm. ....	31
<b>Figure 9.</b> Limiting amount-activity curves.....	33
<b>Figure 10.</b> Determination of the optimal amount and activity. ....	34
<b>Figure 11.</b> Optimal amount and activity and BEDs for the tumour lesions calculated for every point of the CLAAC for two representative virtual patients. ....	39
<b>Figure A - I.</b> Fit of tumour dose factors for $^{177}\text{Lu}$ -DOTATATE based on tumour mass. .....	59

## LIST OF TABLES

<b>Table I.</b> Relevant abbreviations for the developed treatment planning algorithm. ....	23
<b>Table II.</b> Patient characteristics. ....	28
<b>Table III.</b> Optimal amounts and activities, and BEDs and absorbed doses for the OARs and tumour lesions for the optimal plans. ....	37
<b>Table IV.</b> BEDs and absorbed doses for the OARs and tumour lesions resulting from simulating the <i>typically</i> administered amount (265 nmol) and activity (7.4 GBq) (molar activity = 28 MBq/nmol) [71, 89] for the created $^{177}\text{Lu}$ -DOTATATE virtual patients. ....	40
<b>Table V.</b> Progression of the oSF through the cycles (for a total treatment of 4 cycles) for the typical and optimal plans with $^{177}\text{Lu}$ -DOTATATE.. ....	41
<b>Table VI.</b> Progression of the oTCP through the cycles (for a total treatment of 4 cycles) for the typical and optimal plans with $^{177}\text{Lu}$ -DOTATATE. ....	42
<b>Table A - I.</b> Dose factors for $^{177}\text{Lu}$ from OLINDA/EXM [44]. ....	58
<b>Table A - II.</b> Reported dose factors for $^{177}\text{Lu}$ for tumour lesions based on tumour mass [84]. ....	59
<b>Table A - III.</b> Molar activities (MA) for the optimal plans and BEDs and absorbed doses (D) for the liver and spleen for the optimal plan and <i>typically</i> delivered plans. ....	60

## LIST OF ABBREVIATIONS

BED	Biologically effective dose
CLAAC	Combined limiting amount-activity curve
CT	Computerised tomography
LAAC	Limiting amount-activity curve
LQ	Linear-quadratic
MA	Molar activity
NET	Neuroendocrine tumour
OAR	Organ at risk
oBED	Overall biologically effective dose
oSF	Overall survival fraction
oTCP	Overall tumour control probability
PBPK	Physiologically-based pharmacokinetic model
PRRT	Peptide-receptor radionuclide therapy
RM	Red bone marrow
ROI	Region of interest
SF	Survival fraction
TAC	Time-activity curve
TIAC	Time-integrated activity coefficient
TCP	Tumour control probability

# 1 INTRODUCTION

Peptide-receptor radionuclide therapy (PRRT) has shown promising results in the treatment of tumours with high expression of somatostatin receptors such as neuroendocrine tumours (NETs) and meningioma, displaying high sensitivity and specificity [1-5]. However, PRRT can produce high renal and red marrow (RM) toxicity, the kidneys usually being the dose-limiting organ in this therapeutic modality [3]. Despite the positive results achieved with PRRT and its high therapeutic potential [3, 6], the routinely applied treatment can be improved by choosing an individually optimised peptide amount and administered activity for each patient, as shown by Kletting et al. [4]. By doing this, an increased therapeutic index (directly associated with the treatment outcome) can be achieved [4]. Previously, a method was presented, which can be applied to determine the optimal peptide amount and activity leading to a maximum tumour-to-kidney biologically effective dose (BED) ratio [4]. This method was applied to optimise the outcome of PRRT with  $^{90}\text{Y}$ -DOTATATE in nine patients, assuming a maximum kidney BED of 20 Gy<sub>2.5</sub> per cycle (for a total of 2 cycles) in the optimisation process and excluding all the combinations of amount and activity leading to RM BEDs higher than 1 Gy<sub>15</sub> [4]. Although the method developed by Kletting et al. [4] represents an important step forward towards individualised treatment planning in PRRT, some additional features are required to achieve clinical applicability:

1. Multiple tumour lesions need to be considered simultaneously.

Individually applying the optimisation process to each considered lesion/metastasis would lead to as many different “optimal” treatment plans as considered lesions. A suitable treatment planning algorithm must consider multiple tumour lesions simultaneously delivering a single plan to apply to the patient. This is of great relevance for patients with multiple lesions/metastases.

2. Multiple potentially dose-limiting organs (e.g. the kidneys and the RM) need to be considered simultaneously.

Although combinations of amount and activity leading to RM BEDs higher than 1 Gy<sub>15</sub> are correctly excluded in the method presented by Kletting et al. [4], this is done after considering only the kidney BED constraint to determine the optimal activity for each peptide amount. As no recalculations (e.g. considering the RM BED constraint) of the optimal activities for the respective excluded amounts are performed, suboptimal treatment plans may be derived.

3. Constraints in the radiopharmaceutical synthesis need to be accounted for.

This characteristic is important in a treatment planning algorithm for PRRT to guarantee that the delivered combinations of amount and activity can be synthesised.

Therefore, the aim of this work was to develop a clinically applicable algorithm for treatment planning in PRRT based on the method presented by Kletting et al. [4]. Furthermore, to demonstrate the applicability and advantages of the developed algorithm, an *in silico* (i.e. based on computational simulations) clinical trial applying the algorithm to  $^{177}\text{Lu}$ -DOTATATE PRRT in nine virtual patients was conducted.

The thesis is structured as follows:

- Background.

Different fundamental concepts used in the presentation of the developed treatment planning algorithm are introduced in this chapter. Firstly, a general overview of molecular radiotherapy (MRT) is given: this includes short descriptions of the characteristics of the used radiopharmaceuticals and of the main applied techniques. In the second and third parts of the Background chapter the concepts of pharmacokinetics and physiologically-based pharmacokinetic (PBPK) models are introduced. A good understanding of these concepts is required as the developed treatment plan algorithm is based on PBPK models. In the fourth part of this chapter, the concepts of dosimetry and BED are explained in detail. These concepts are also fundamental to correctly understand the developed algorithm as BED constraints are to be considered to achieve treatment plans that can be safely applied to the patients. Lastly, the current state of treatment planning in MRT is presented to put the developed treatment planning algorithm in context.

- Presentation of the developed treatment planning algorithm.

In this section the developed concepts of overall BED (oBED) and overall tumour control probability (oTCP) are described. In addition, the concept of virtual patient is described and the characteristics of the virtual patients (i.e. characteristics of the patients and of the PBPK model) used in the conducted *in silico* clinical trial are presented. Lastly, in this section, the general workflow of the developed treatment planning algorithm is given, which is the most important part of the whole manuscript.

- *In silico* clinical trial.

In this section, optimal plans are obtained by applying the developed treatment planning algorithm to simulations of pharmacokinetics with  $^{177}\text{Lu}$ -DOTATATE using nine virtual patients. Subsequently, the derived optimal plans and a *typically* delivered plan for  $^{177}\text{Lu}$ -DOTATATE are compared considering tumour BED values and values for the developed concept of oTCP.



## **2 BACKGROUND**

### **2.1 Molecular Radiotherapy**

Molecular radiotherapy (MRT) is a predominantly systemic therapy for the treatment of cancer in which a radiopharmaceutical or radionuclide is administered to patients to kill or sterilise tumour cells [7]. This kind of therapy, which has been already used for more than 50 years, exploits biological and physiological differences between the tumours or tumour-host tissues and the normal tissues to increase the accumulation of the radiopharmaceutical [8-10]. Therefore, the radiation absorbed dose, in a region of interest (i.e. the tumour or tumour-host tissue) [8-10]. MRT has been used for the treatment of multiple types of cancer, for both primary tumours and metastases [11, 12]. The most commonly used mechanism in MRT is to administer radiopharmaceuticals which target peptide-receptors (peptide-receptor radionuclide therapy (PRRT)) or antigens (radioimmunotherapy) overexpressed in tumour cells [8, 9, 11, 13, 14]. Specific characteristics of the tumour-host tissue have also been exploited to generate higher accumulation of the radiopharmaceutical or radionuclide in the region of interest [10, 11, 15]. Radioactive iodine, for example, has been used for thyroid cancer treatment as thyroid cells have a high uptake of iodine to produce hormones [10, 11, 15]. However, as MRT is a systemic therapy and the targeted antigens, receptors or cellular mechanisms may be presented not exclusively on the tumours or tumour-host tissues, MRT may also produce considerable damage to normal tissues. Furthermore, the biodistribution of the radiopharmaceuticals over time (i.e. pharmacokinetics) is patient-specific because of inter-individual anatomical and physiological differences [4, 7, 16-19]. Therefore, the main challenges in MRT are:

- a) Synthesis of radiopharmaceuticals with high accumulation in the target tissue/cells (i.e. tumour or tumour-host tissue/cells) and low accumulation in normal tissues/cells.
- b) Individualised treatment planning aiming at maximising the number of killed/sterilised tumour cells while avoiding high toxicity to normal tissues for a given radiopharmaceutical.

#### **2.1.1 Radiopharmaceuticals in Molecular Radiotherapy**

Radiopharmaceuticals consist of two main components: a carrier and a radionuclide [20]. The carrier is usually a substance with high affinity to tumour-associated target molecules which allows high accumulation in the tumour region or tumour-host tissue [11, 20]. The most frequently used carrier molecules are: small molecules, peptides, proteins and antibodies [20, 21]. The radionuclide is attached to the carrier and emits radioactive particles which can kill/sterilise tumour cells by producing direct or indirect DNA damage [22]. Emitters of  $\alpha$  particles,  $\beta$  particles or Auger electrons are used for

therapy [20]. Nuclides emitting  $\gamma$  radiation or positrons can also be attached to carriers but these are mostly used for imaging purposes [20]. Some nuclides allow both therapy and imaging as they produce more than one type of emission (e.g.  $^{177}\text{Lu}$  emits  $\beta^-$  particles (used for therapy) and  $\gamma$  radiation (used for imaging) [3, 14, 20]). The radioactivity (i.e. activity) of a nuclide is determined by its radioactive half-life  $T_{1/2}$  which is the time in which the number of radiation decays (i.e. disintegrations) per second is reduced to half its initial value. Nuclides with long radioactive half-lives (e.g.  $^{90}\text{Y}$  (64.8 h) and  $^{177}\text{Lu}$  (153.6 h)) are commonly used for therapy while nuclides with short radioactive half-lives (e.g.  $^{68}\text{Ga}$  (67.6 min) and  $^{18}\text{F}$  (110 min)) are more common for imaging [23].

Multiple combinations of carrier molecules and nuclides are used in molecular radiotherapy [12]. To label carrier molecules with radionuclides two main methods are used: direct and indirect labelling [21]. Direct labelling consists in modifying the carrier molecule to create binding sites for the radionuclide [21]. Indirect labelling consists in using additional structures which bind to both the carrier and the radionuclide, acting as a bridge between them [21]. The used labelling method depends on the properties of both the radionuclide and the carrier [24]. Examples of direct and indirect labelling are presented in Figure 1 [24].

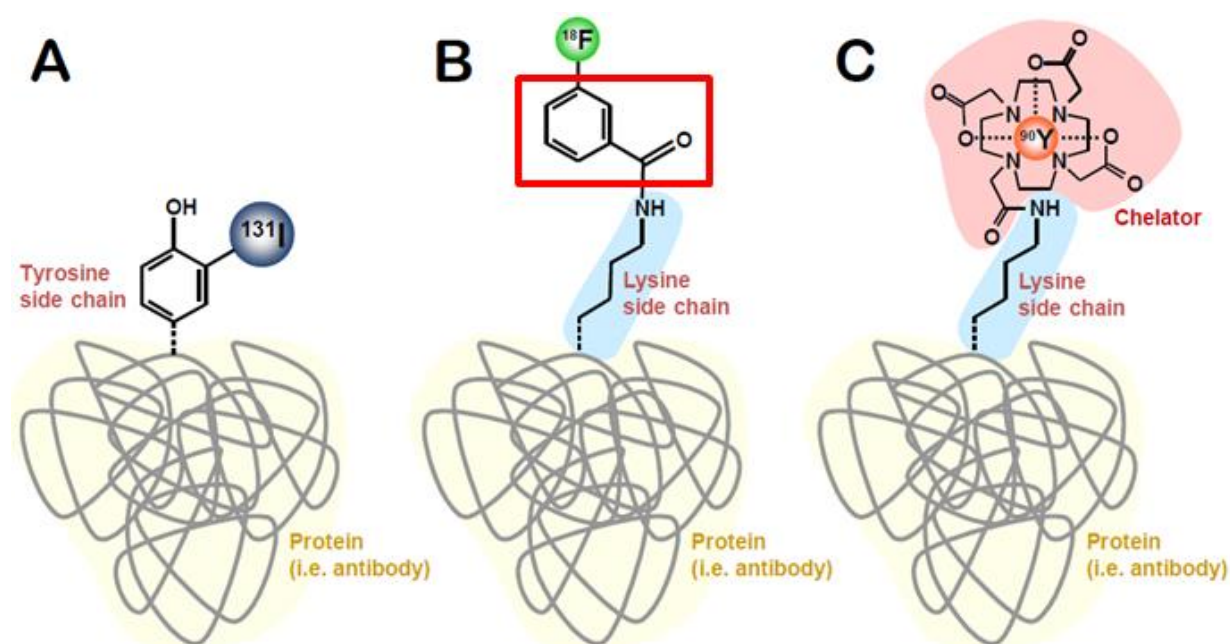


**Figure 1.** Labelling techniques [24]. A: Direct labelling. The  $^{131}\text{I}$  radionuclide (dark blue) is directly attached to a modified section (side chain) of the carrier. B: Indirect labelling using an additional structure. The  $^{18}\text{F}$  is first attached to an additional structure (red) which also binds the carrier. C: Indirect labelling using chelators. A chelator (light red region) is a special molecular construction mostly used for labelling with metallic radionuclides (e.g.  $^{90}\text{Y}$  (orange)) [24].

In practice, not all the carrier molecules can be labelled during the synthesis of therapeutic radiopharmaceuticals (usually < 5 % of carriers are labelled). This generates, in principle, two kinds of substances: labelled and unlabelled carriers, which compete for the available target molecules (this competition is described by nonlinear equations). Moreover, radionuclides are produced with an activity which is limited depending on the nuclide itself and on the production technique [25]. These factors limit the maximum achievable molar activity (i.e. activity per mole of radiopharmaceutical) which is proportional to the maximum achievable specific activity (i.e. activity per gram of radiopharmaceutical) [26]. Molar activity is usually measured in units of [MBq/nmol] and specific activity in units of [MBq/μg] [25, 26].

### 2.1.2 Peptide-Receptor Radionuclide Therapy

As some tumours overexpress peptide-receptors, peptides with high affinity to the overexpressed receptors which are labelled with therapeutic radionuclides (i.e.  $\alpha$ ,  $\beta$  and or Auger electron emitters) are used for the treatment of these kinds of tumours [20]. Molecular radiotherapy using labelled peptides to target the corresponding peptide-receptors in the tumour cells is called peptide-receptor radionuclide therapy [3, 13]. This radiotherapy technique is relatively new, as it was first introduced in the 1990s [3]. In PRRT,  $\beta^-$  emitters (e.g.  $^{90}\text{Y}$  and  $^{177}\text{Lu}$ ) are commonly used for labelling peptides [3, 13, 14]. However, other kinds of radionuclides (e.g.  $^{111}\text{In}$ , an Auger electron emitter) are also utilised in practice [3, 12, 27]. The most explored targeted peptide-receptors in PRRT are the group of somatostatin receptors (SSTR), with the SSRT type 2 (SSRT2) being of great interest due to its high expression in neuroendocrine tumours (NETs) and other tumours of the nervous system (e.g. meningioma and neuroblastoma) [3, 5]. Other receptors that have been targeted in PRRT are for example the gastrin-releasing peptide receptors (GRPRs), which overexpress in gastrointestinal tumours [28, 29].

According to the effect produced by the drug-receptor interaction, carrier peptides can be classified as [30, 31]:

- **Full agonists:** produce the same biological response as the native peptide.
- **Partial agonists:** produce a fraction of the biological response produced by the native peptide.
- **Superagonists:** produce a higher biological response than the native peptide [31].
- **Antagonists:** do not produce any biological effect and only make the bound peptide-receptors unavailable for other molecules.
- **Inverse agonists:** produce a partial or full biological response opposite to the native peptide response.

Antagonist carrier peptides may be desirable as they do not produce complex biodynamic interactions (i.e. modifications of metabolic functions) which could

generate adverse side effects [30, 32, 33]. In addition, although peptide antagonists do not undergo specific internalisation, which could reduce their accumulation in the target tissue, the superiority of SSTR2-antagonist radiopharmaceuticals has been demonstrated [33].

Two of the most commonly used carrier peptides in PRRT are [DOTA0,Tyr3]-octreotide (DOTATOC) and [DOTA0,Tyr3,Thr8]-octreotide or [DOTA0,Tyr3]-octreotate (DOTATATE) [3, 13, 14]. These peptides are both SSRT2 agonists [3, 33]. For these two radiopharmaceuticals, DOTA indicates the used bifunctional chelating molecule (i.e. binds both the carrier and the radionuclide) and the rest of the name description corresponds to the modified carrier molecule [3]. DOTATOC and DOTATATE are usually labelled with  $^{90}\text{Y}$  or  $^{177}\text{Lu}$  for therapy and with  $^{68}\text{Ga}$  and  $^{111}\text{In}$  for imaging [3, 13, 14].

Although PRRT has shown promising results, especially in the treatment of tumours with high expression of SSTRs (e.g. NETs and meningioma), this therapeutic technique may produce high renal and red marrow (RM) toxicity, the kidneys usually being the dose-limiting organ [1-5, 34]. Therefore, to reduce the nonspecific uptake of radiopharmaceutical in the kidneys, a solution of amino acids (e.g. lysine and arginine) is routinely co-administered before the infusion of the radiopharmaceutical [35].

### **2.1.3 Radioimmunotherapy**

Molecular radiotherapy performed with labelled antibodies targeting antigens overexpressed in the tumour cells is called radioimmunotherapy (RIT) [18]. This therapeutic modality, used for more than 50 years, can be administered intravenously but also intracavitary, e.g. in the peritoneum [8, 9]. RIT has been used mostly for the treatment of haematological malignancies (e.g. leukaemia or lymphoma) but can also be used to treat solid tumours [8, 9]. In addition, RIT has been applied for immunosuppression (i.e. weakening of the immune system to avoid immune reactions, e.g. as preparation for stem cell transplant) [18]. Some of the targeted antigens in RIT are the haematopoietic cluster of differentiation (CD) antigens (e.g. CD33, CD45 and CD66) for different types of leukaemia, and the prostate-specific membrane antigen (PSMA) for prostate cancer [8, 17, 19]. In RIT, the usual organs at risk (OARs) are the red marrow, the kidneys, the salivary glands and the liver [18, 19, 36]. However, the dose-limiting organ in RIT depends on the selected antibody and nuclide and on patient-specific pharmacokinetics [16, 37].

According to their origin, antibodies can be classified as monoclonal and polyclonal antibodies [38]. Monoclonal antibodies (mAbs) are produced from a single B lymphocyte clone and are therefore all identical [38]. As a consequence, mAbs target the same antigen and the same epitope (i.e. binding site in the antigen) [38]. Polyclonal antibodies (pAbs), in contrast, are produced from different B lymphocytes

which recognise the same antigen and hence, they are not homogenous [38]. Thus, pAbs bind the same antigen but at different epitopes [38]. Because of the higher specificity of mAbs (they target the same epitope in the same antigen), mAbs have been the standard selection for the treatment of cancer for more than 20 years [39].

A special modality of RIT is pretargeted radioimmunotherapy (PRIT). PRIT, introduced in the 1980s, is a two- or multistep technique, which fundamentally consists in administering the antibody molecules and the nuclide molecules independently [12]. First, the antibody molecules with additional binding structures are administered [12]. After some time, in which it is expected that the antibodies (with the additional structures) are mostly cleared from the blood and attached to the antigens, the radioactive molecules are administered [8]. The administered radioactive molecules have extra structures with high affinity to the structures added to the antibodies. Consequently, the radioactive molecules will bind the antibodies bound to the antigens (Figure 2, A) [40].

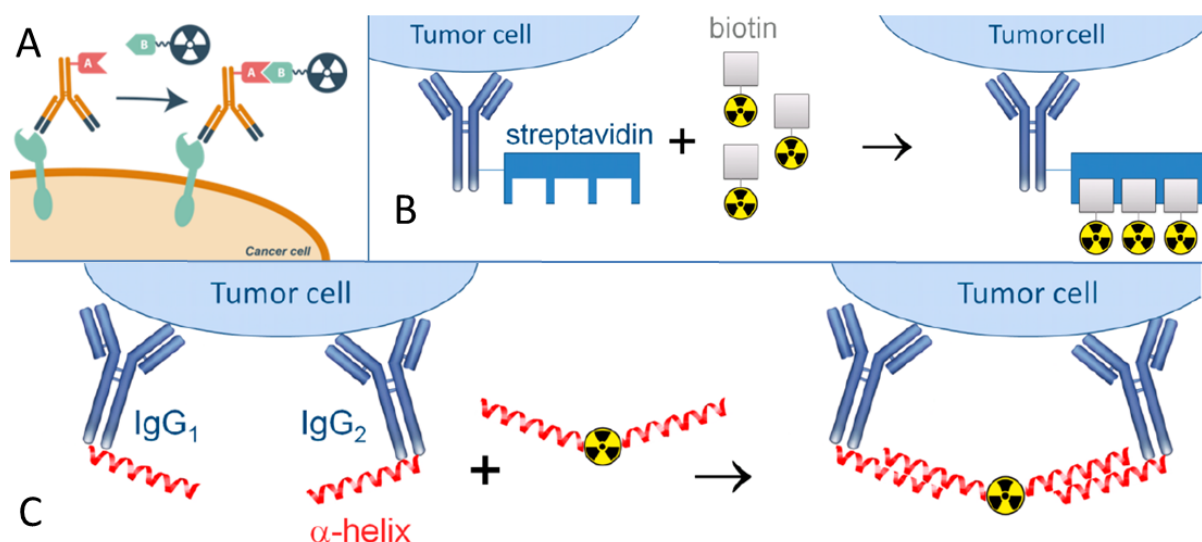


**Figure 2.** Pretargeted radioimmunotherapy. A) Pretargeted radioimmunotherapy in which one radioactive molecule with additional structure B binds one previously administered antibody with additional structure A bound to the antigen in the tumour cell. The additional structures A and B are complementary or have a very high affinity between them [40]. B) Pretargeted radioimmunotherapy enhancing the number of radioactive molecules per bound antibodies. In this configuration, the additional structure in the antibody can bind multiple radioactive molecules [12]. C) Pretargeted radioimmunotherapy with increased specificity due to the stronger binding (double binding) to the antibodies [12].

PRIT is used to improve the therapeutic index (i.e. the ratio between the tumour absorbed dose and the absorbed dose in the dose-limiting organ, e.g. the red marrow) and to reduce the overall absorbed dose in the body. An overall absorbed dose reduction is achieved as the small radioactive molecules rapidly penetrate the tumour site where are highly bound to the modified antibodies [8, 9, 12]. In addition,

the unbound radioactive molecules are easily excreted in the urine which lowers the overall absorbed dose to the OARs and to the body [8]. Furthermore, using this technique allows to attach multiple radioactive molecules to a bound antibody (producing a higher therapeutic effect) or to increase the specificity by binding a radioactive molecule to more than one bound antibody (Figure 2, B and C) [12].

## 2.2 Pharmacokinetics

Pharmacokinetics (also called drug biokinetics or simply biokinetics) is the study of the absorption, distribution, metabolism and excretion (ADME) over time of a pharmaceutical (or radiopharmaceutical) administered to an organism [37, 41]. Pharmacokinetics depends on multiple factors such as drug-specific, organism-specific and administration-specific characteristics, which determine the ADME for different scenarios and individuals.

Absorption is the process in which the administered pharmaceutical passes from the administration site to the blood [37, 41]. The process of absorption applies mostly for orally administered drugs (or indirectly administered drugs) which can be eliminated through the gastrointestinal tract (or through other ways) before reaching the main bloodstream [37]. Therefore, for orally administered drugs, the concept of drug bioavailability (i.e. fraction of the administered drug, which reaches the main bloodstream) is of relevance [37, 41]. For intravenously administered drugs, the concept of absorption, and therefore bioavailability, is not of high relevance as the pharmaceutical is administered directly to the bloodstream (in principle, 100 % bioavailability). However, binding of the pharmaceutical to some serum proteins (e.g. albumin) or to erythrocytes can reduce the effective available fraction of the administered drug (i.e. effective bioavailability) [37, 42].

Distribution is the process in which the bioavailable pharmaceutical passes from the main bloodstream to the organs and tissues [37, 41]. Distribution directly depends on the blood/plasma volume in the central circulatory system, the organ/tissue blood flow (or plasma flow) and the vascular volume (i.e. the amount of blood/plasma in an organ or tissue). These parameters determine the drug transfer rate (in units or subunits of  $[\text{min}^{-1}]$ ) from the main bloodstream to the organs/tissues and from the organs/tissues back to the main bloodstream [4]. An additional process involved in the distribution of a pharmaceutical is permeability. In simple words, permeability can be defined as the amount of drug passing from the organ vascular volume, also called vascular space, to the organ interstitium (i.e. space around the organ cells). This process is highly important for most pharmaceuticals because if a drug does not reach the organ interstitium it cannot interact with the organ cells.

Metabolism, for a pharmaceutical, is the decomposition of a molecule in submolecules allowing/facilitating further interactions or excretion [37]. The main metabolic organ is the liver, however, other organs/tissues such as the intestines, the

kidneys, the lungs, the brain and the blood can perform metabolic functions [37]. The submolecules resulting after a metabolic process are called metabolites.

Excretion is an elimination process in which waste substances are taken outside of an organism (e.g. to the intestines or the bladder). Once a pharmaceutical enters the main bloodstream, it will be mostly excreted by the kidneys through the urine or by the liver through the bile, which is subsequently eliminated through the stools [37, 41].

For radiopharmaceuticals labelled with a nuclide which allows imaging (e.g.  $^{18}\text{F}$ ,  $^{68}\text{Ga}$ ,  $^{111}\text{In}$  or  $^{177}\text{Lu}$ ), the pharmacokinetics in different organs/tissues can be determined/estimated using series of radiation-based images (e.g. positron-emission tomography (PET), single-photon emission computed tomography (SPECT) or gamma camera images). Radiopharmaceuticals sharing the same carrier (e.g.  $^{68}\text{Ga}$ -DOTATATE,  $^{177}\text{Lu}$ -DOTATATE and unlabelled DOTATATE) are usually assumed to have the same pharmacokinetic characteristics. The activity measured in the organ/tissue varies over time because of the drug pharmacokinetics and the nuclide radioactive decay. The activity measured in a tissue at a time-point is closely related to the amount of radiopharmaceutical in the tissue at that specific time. The graphical representation of the variation of the activity over time in a region of interest (e.g. organ, tissue, blood or whole body) is called time-activity curve (TAC) (Figure 3). TACs are sometimes presented in relative units of activity (e.g. [MBq/g], [MBq/ml], % injected activity, % injected activity/ml) as the data retrieved from radiation-based images (e.g. PET, SPECT and gamma camera images) and blood activity measurements are usually given in relative units. The area lying below a TAC is called area under the curve (AUC) and represents the total amount of radiation produced by the radiopharmaceutical accumulated over time (i.e. time-integrated activity, in units of [Bq·s] [43]) in a tissue. However, this is only valid when the TAC is represented in absolute units of activity (e.g. [MBq]) (Figure 3). The AUC can thus be used to calculate the absorbed dose in the tissue [44]. However, the absorbed dose in a tissue does not only depend on the amount of radiation produced in the specific tissue but also on radiation generated in surrounding tissues [44, 45]. Thus, more complex dosimetric calculations are to be performed to determine the total absorbed dose in the organs/tissues [44].

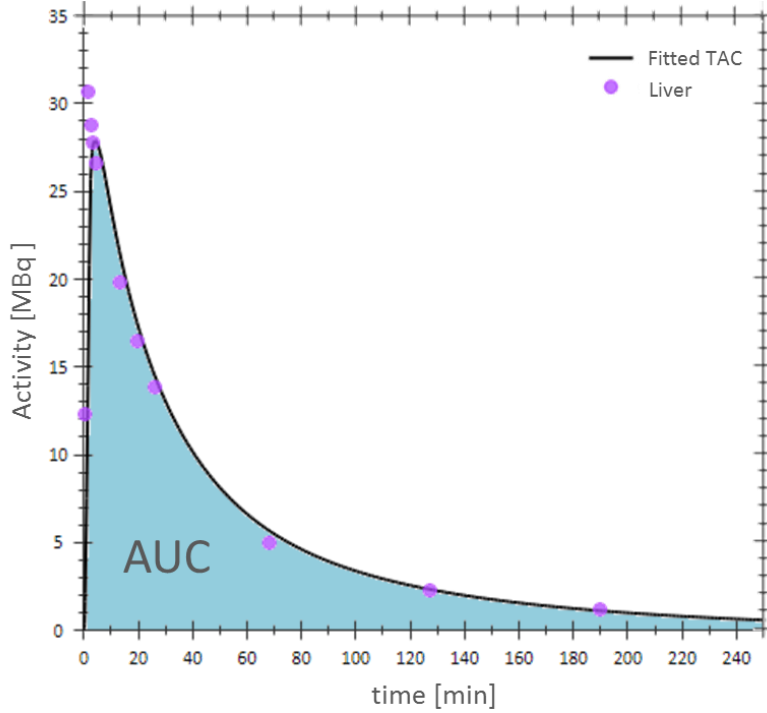


**Figure 3.** Time-activity curve and area under the curve. The activity measurements retrieved from a series of radiation-based images (purple dots) are used to generate a fitted time-activity curve (TAC) (black solid line). The area under the curve (AUC) (light blue) is the region lying below the fitted TAC. Example data from a female patient of 67 kg after a bolus administration of 178.5 MBq (32 nmol) of  $^{68}\text{Ga}$ -NeoBOMB1.

As the amount of measured data points is limited, TACs are usually generated by fitting a sum of exponential functions to the measured data (Eq. (1)). Exponential functions are used as both the radioactive decay and most biological processes follow exponential kinetics [46]. TACs expressed as fitted functions allow prediction of the activity for time-points not considered during the imaging protocol, such as intermediate time-points and time-points after the last measured data point. Fitted TACs also allow to perform better calculations/estimations of the AUC by integrating the TACs from time zero to infinity. As the radioactive decay rate ( $\lambda_{phy}$ ) is a known parameter ( $\lambda_{phy} = \ln(2)/T_{1/2}$ , where  $T_{1/2}$  is the half-life of the radioactive nuclide), the fitting function used for the TACs is usually presented as [46]:

$$A(t) = \sum A_i \cdot e^{-(\lambda_{phy} + \lambda_i) \cdot t} \quad (1)$$

where  $A(t)$  is the activity over time,  $A_i$  values are linear coefficients and  $\lambda_i$  values are exponential coefficients. The fitting process consists in obtaining the  $A_i$  and  $\lambda_i$  values better supported by the measured data [46]. However, the number of exponential functions used to fit a TAC to the data is not fixed (e.g. TACs can be fitted using one, two, three or more exponential functions). Therefore, to avoid over- or underfitting of the data, the Akaike information criterion (AIC) is used [46]. AIC is a statistical analysis used to determine the likelihood of a model (e.g. a function) among a group of models being best supported by the measured data [46]. AIC considers the



differences between the fitted function and measured data (in this case, the sum of squared errors (SS)) as well as the number of parameters (e.g.  $A_i$  and  $\lambda_i$  values) and the number of data points [46]. Thus, AIC is used to determine the optimal number of exponential functions to use for fitting each TAC [46]. AIC is also used with more complex systems such as physiologically-based pharmacokinetic (PBPK) models to determine the PBPK model best supported by the measured pharmacokinetic data.

## 2.3 PBPK Models

A physiologically-based pharmacokinetic (PBPK) model is a compartment-based mechanistic model used to describe drug pharmacokinetics [47]. What differentiates PBPK models from other mechanistic pharmacokinetic models is the use of anatomical, physiological and drug-specific parameters, which makes PBPK models the most comprehensive type of pharmacokinetic models [47]. The constitutive compartments of a PBPK model represent anatomical or functional regions of interest (ROIs) which can be defined by considering a group of organs/tissues, a single whole organ/tissue or a subpart of an organ/tissue. The value of a compartment at a specific time-point corresponds, directly or indirectly, to the amount of the modelled substance at that particular time in the region represented by the compartment. The connections between compartments are defined by physiological connections between organs or tissue regions (e.g. blood flows) and represent the transfer rates of the drug from one compartment to another. The values of the transfer rates in a PBPK model, in units or subunits of  $[\text{min}^{-1}]$ , are calculated based on anatomical, physiological and drug-specific parameters. Depending on the complexity of the PBPK model, some of or all the following parameters can be considered to determine the model transfer rates: vascular volumes, plasma flows, permeability values, interstitium volumes, intracellular volumes, association rates (i.e. binding rates), dissociation rates (i.e. unbinding rates), metabolic rates, receptor/antigen densities, receptor/antigen synthesis rates, receptor/antigen degradation rates, receptor/antigen recycling rates, nonspecific uptake rates, internalisation rates and excretion rates [4]. For PBPK modelling of radiopharmaceuticals, labelled and unlabelled (or radioactive and nonradioactive) substances are independently considered in the model and are connected by the radiation decay rate  $\lambda_{phy}$ . Labelled and unlabelled substances are usually assumed to have the same pharmacokinetics [4], even though they have different molecular structures and therefore different pharmacokinetic characteristics (e.g. affinity and permeability). Labelled and unlabelled substances compete in a nonlinear manner for the available target molecules.

The simplest PBPK model (considering not only the central circulatory system) is a two-compartment model, which is usually represented by a schematic such as in Figure 4.

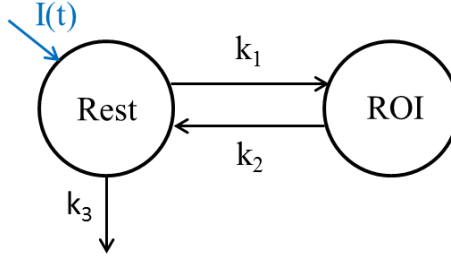


**Figure 4.** Two-compartment PBPK model. Compartments are represented by circles and transfer rates by arrows indicating the transfer direction of the substance. The right-hand side compartment represents a region of interest (ROI) and the left-hand side compartment represents the rest of the body. The parameter  $I(t)$  represents the drug administration function (i.e. input function). The parameter  $k_1$  is the transfer rate from the rest of the body to the ROI,  $k_2$  is the transfer rate from the ROI to the rest of the body and  $k_3$  is the excretion rate.

Two differential equations mathematically describe the two-compartment PBPK model presented in Figure 4 and are formulated as follows [48]:

$$\frac{dA_{Rest}(t)}{dt} = \frac{dI(t)}{dt} - k_1 \cdot A_{Rest}(t) + k_2 \cdot A_{ROI}(t) - k_3 \cdot A_{Rest}(t) \quad (2)$$

$$\frac{dA_{ROI}(t)}{dt} = k_1 \cdot A_{Rest}(t) - k_2 \cdot A_{ROI}(t) \quad (3)$$

where  $A_{Rest}(t)$  is the amount of substance in the rest of the body,  $A_{ROI}(t)$  is the amount of substance in the ROI,  $I(t)$  is the input function and  $k_1$ ,  $k_2$  and  $k_3$  are the transfer rates as described in Figure 4. For administering a total amount of substance  $A_0$  using an intravenous bolus administration schedule (i.e. instant administration; in practice, administration in  $< 3$  min), it can be assumed that  $dI(t)/dt = 0$  and that the initial conditions to solve the system of differential equations are:  $A_{Rest} = A_0$  and  $A_{ROI} = 0$  [48]. For administration schedules using a constant administration rate  $R_0$ , it can be assumed that  $dI(t)/dt = R_0$  during the administration time and zero otherwise, and that the initial conditions are:  $A_{Rest} = 0$  and  $A_{ROI} = 0$ . Varying administration schedules can also be applied. For drugs indirectly administered (e.g. orally) the bioavailability over time needs to be considered to determine the input function  $I(t)$ .

More complex PBPK models considering multiple organs and subparts of the organs have been developed to achieve a higher descriptiveness of the pharmacokinetics [4]. These PBPK models require the solution of more complex systems of differential equations (sometimes nonlinear systems). A whole-body PBPK model considering multiple organs and subparts of the organs is shown in Figure 5 [4].

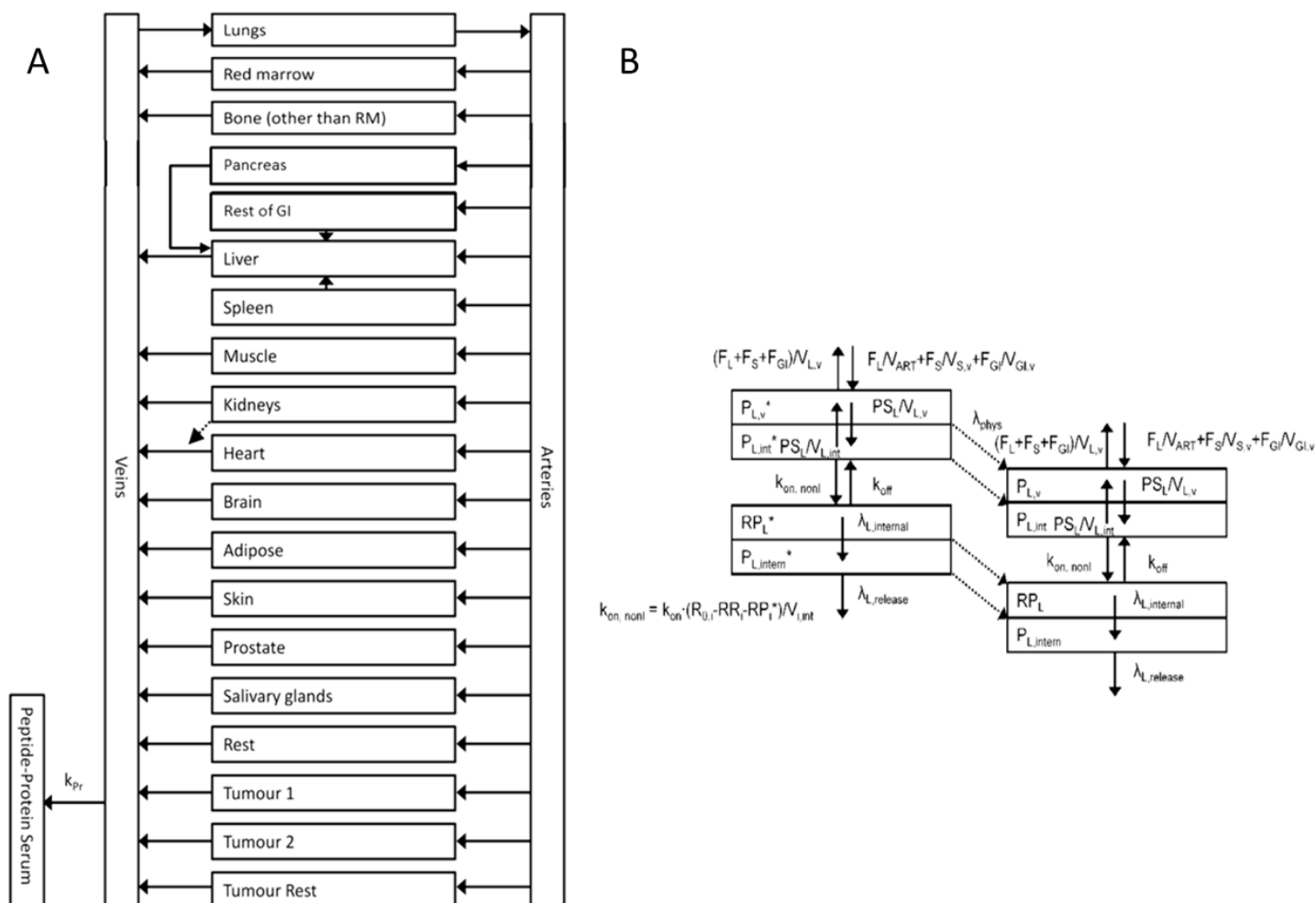


**Figure 5.** Whole-body PBPK model [4]. A) Main structure of the PBPK model. The organs are connected via the blood flow according to the human physiology. The model considers the arterial and venous circulatory systems independently and considers, in addition, the binding of the substance to serum proteins. B) Modelling of the organ subparts. Individual compartments for the vascular space, interstitial space, cellular membrane and intracellular space are considered for most organs. Transfer rates are based on physiological and drug-specific parameters. Labeled (left) and unlabeled (right) substances are independently considered and are linked by the radiation decay rate  $\lambda_{phys}$ .

Ideally, all the parameters of a PBPK model are known for each individual. However, in practice, many parameters are unknown or, in a better case scenario, known for a group of individuals of the same species or of another species. In addition, some parameters may present a large inter-individual biological variability [16]. Therefore, some model parameters are estimated using allometric scaling or need to be fitted (best individually) to measured data [16]. Allometric scaling consists in estimating anatomical and physiological parameters based on data from the same or different species [49]. Three main types of parameters are used to fit a PBPK model to measured data: fixed, adjustable and Bayes parameters [50]. Fixed parameters are used when there is a high certainty about the parameter value. Adjustable parameters are used when nothing or very little is known about the parameter. Bayes

parameters (i.e. based on a known distribution) are used when data from a group of individuals is available [51]. However, for some authors, defining which parameters need to be considered as fixed, adjustable or Bayes when fitting a PBPK model to measured data can be considered an art form. Nowadays, there are specialised pieces of software which facilitate the processes of building PBPK models and fitting them to measured data (e.g. SAAM II [50]).

Once a PBPK model is validated with measured data, simulations of pharmacokinetics varying several parameters such as the administered amount of pharmaceutical or the administration schedule can be performed. The possibility of performing simulations of diverse scenarios allows the use of PBPK models for multiple purposes such as improving imaging protocols, planning therapy, optimising clinical trials and performing *in silico* clinical trials [52]. In addition, for radiopharmaceuticals with the same carrier and assuming the same pharmacokinetics, a PBPK model generated with data for one radiopharmaceutical (e.g.  $^{111}\text{In}$ -DOTATATE) can be easily adapted to another radiopharmaceutical (e.g.  $^{177}\text{Lu}$ -DOTATATE) by changing the radioactive decay rate  $\lambda_{\text{phy}}$ . This increases the applicability of PBPK models.

## 2.4 Dosimetry in Molecular Radiotherapy

As indicated by its name, dosimetry consists in measuring dose. Dosimetry in molecular radiotherapy is also called internal dosimetry as the radiation is produced inside the body. In MRT two kinds of doses are of relevance: radiation absorbed dose (i.e. amount of deposited energy in a tissue) and biologically effective dose (BED) (i.e. representation of dose accounting for the biological effect in a tissue) [53]. The calculation of the BED considers the radiation absorbed dose in the tissue, the sensitivity of the tissue to the specific kind of radiation and the tissue repair during the radiation exposure. Thus, the correctness of the BED calculations depends on the measurement accuracy of the radiation absorbed doses. In MRT, dosimetry of the radiation absorbed dose (also called absorbed dose or physical dose) consists of two main steps:

1. Measurement of the time-integrated activity values produced by the radiopharmaceutical accumulated in the ROIs (e.g. in the main organs and tissues) [45].
2. Calculation of the absorbed doses based on the time-integrated activity measurements in the ROIs.

The measurement of the activity, and therefore the calculation of the time-integrated activity, in the ROIs is founded on quantitative radiation-based images (e.g. PET, SPECT or gamma camera images). From these images, the total amount of radioactive emissions generated by the radiopharmaceutical over a period of time in each ROI (e.g. an organ/tissue) can be determined. However, to achieve accurate

quantification, multiple correction factors are to be applied to the images [45, 54]. The most relevant corrections applied to quantitative radiation-based images are: attenuation correction, dead-time correction, sensitivity correction, background correction and scatter correction [45, 54]. Attenuation correction accounts for the produced radiation emissions which are absorbed in the imaged object (e.g. the body) and therefore do not reach the radiation detectors. Dead-time correction needs to be performed when the time interval between radiation emissions reaching a radiation detector is shorter than the processing time capacity of the system. Dead-time correction is therefore of high relevance for high-activity measurements [45, 54]. The correction for the sensitivity of a radiation detector system consists in ensuring accurate transfer functions associating the received events with the delivered activity values. The sensitivity of a detector system depends on the energy and type of the measured radiation. Therefore, the type of nuclide used needs to be considered when defining the system transfer functions to use during image reconstruction [45, 54]. Background correction considers the radiation emissions produced in regions adjacent to the ROI, which may alter the resulting measurements. Scatter correction accounts for the trajectory deviations of the radiation emissions produced by the interaction with the matter of the imaged object. The corrected activity data are subsequently used to generate TACs and to calculate the time-integrated activity in the ROIs [45].

Time-integrated activity values are then used to calculate the absorbed doses in the ROIs. The calculation of the absorbed dose in a ROI considers radiation produced both in the respective ROI and in other ROIs. Thus, ROIs can be classified as source regions (i.e. where radiation is produced) and target regions (i.e. where radiation is absorbed). The radiation characteristics, the mass of the target region and the spatial distribution of the source region ( $rS$ ) and the target region ( $rT$ ) define factors to determine the absorbed dose in the target region per unit of activity in the source region  $S_{(rT \leftarrow rS)}$  (also called dose factors or S values) [43, 55].

Time-integrated activity values can also be normalised by dividing them by the administered activity  $A_0$  (in units of [Bq]). Normalised time-integrated activity values are called time-integrated activity coefficients (TIACs). Thus, based on the time-integrated activity value in a source region  $\tilde{A}_{rS}(T)$  (in units of [Bq·s]), the TIAC in a source region  $\tilde{a}_{rS}(T)$  (in units of [s]) is defined as:

$$\tilde{a}_{rS}(T) = \frac{\tilde{A}_{rS}(T)}{A_0} \quad (4)$$

where  $T$  is the radiation exposure time. TIACs were formerly called residence times because of their temporal units. Using the factors  $S_{(rT \leftarrow rS)}$  (in units of [Gy/Bq]) between the target region and the considered source regions, the injected activity  $A_0$  and the TIACs  $\tilde{a}_{rS}(T)$  for all the considered source regions, the absorbed dose rate (i.e. dose rate) and the absorbed dose in a target region are defined as:

$$\dot{D}_{rT}(t) = A_0 \cdot \sum_{rS=1}^N a_{rS}(t) \cdot S_{(rT \leftarrow rS)} \quad (5)$$

$$D_{rT}(T) = A_0 \cdot \sum_{rS=1}^N \tilde{a}_{rS}(T) \cdot S_{(rT \leftarrow rS)} \quad (6)$$

where  $\dot{D}_{rT}(t)$  is the dose rate over time in the target region (in units of [Gy/s]) and  $D_{rT}(T)$  is the absorbed dose in the target region after the exposure time  $T$  (in units of [Gy] = [J/kg]). The subscripts  $rS$  and  $rT$  respectively stand for source region and target region, while  $N$  is the number of considered source regions. The parameter  $a_{rS}(t)$  is the fraction of the administered activity over time for each source region. The factors  $S_{(rT \leftarrow rS)}$  are specific for each nuclide and for each combination of source region and target region. Therefore, tables with values for  $S_{(rT \leftarrow rS)}$ , in which the source and target regions are different body organs/tissues, are available in the literature and are incorporated in software used for internal dosimetry (e.g. OLINDA/EXM) [44, 56]. The TIACs ( $\tilde{a}_{rS}(T)$  values) of the considered ROIs are the common input values for internal dosimetry software. A TIAC for the rest of the body (i.e. the total body excluding the selected ROIs) should also be calculated and entered as an input value [44]. Some additional features such as the frequency of bladder voiding can be considered too when performing dose calculations in some pieces of software for internal dosimetry.

#### 2.4.1 Biologically Effective Dose

Ionising radiation absorbed in tissue can produce direct or indirect DNA damage [57]. Direct damage is produced when ionising radiation interacts with DNA molecules resulting in bond breaks [57]. Indirect DNA damage is produced when ionising radiation interacts with molecules adjacent to the DNA structure generating free radicals which subsequently interact with the DNA producing bond breaks [57]. Single- (SSB) or double- (DSB) strand breaks can occur in the DNA structure after interaction with ionising radiation. However, there are several cell mechanisms that allow complete or partial DNA repair of both SSB and DSB [58]. Depending on the produced DNA damage, an irradiated cell can completely recover, be sterilised (i.e. cannot further proliferate but it is still functional), mutate or undergo apoptosis (i.e. cell death) [58]. Strand breaks can produce cell death when the repair mechanisms cannot repair the DNA damage (DSB are more likely to produce cell death than SSB) [57, 59]. Several models have been used to describe the effect of radiation on cells, among which the linear-quadratic (LQ) model is the most commonly accepted and used one [60]. The LQ is a mechanistic model that describes the fraction of cells that survive after exposure to ionising radiation (i.e. survival fraction (SF)) [60]. Thus, SF values represent the probability of survival for a cell after radiation exposure. Four main parameters are considered in the LQ model for the calculation of the SF: absorbed dose, lethal damage (i.e. cell kill produced by a single radiation emission, also called single-hit cell kill), sub-lethal damage (i.e. cell kill produced by different

radiation emissions) and the relationship between damage repair rate and dose rate [53, 61]. Thus, according to the LQ model, SF is described as:

$$SF = e^{-\alpha \cdot D - G \cdot \beta \cdot D^2} \quad (7)$$

where  $\alpha$  (in units of  $[\text{Gy}^{-1}]$ ) is the parameter accounting for lethal damage,  $\beta$  (in units of  $[\text{Gy}^{-2}]$ ) is the parameter taking into account the sub-lethal damage,  $G$  is the Lea-Catcheside factor representing the relationship between dose rate and repair rate and  $D$  is the absorbed dose [60]. The  $G$  factor is defined as:

$$G(T) = \frac{2}{D^2} \cdot \int_0^T \dot{D}(t) \cdot \left( \int_0^t \dot{D}(w) \cdot e^{-\mu_{rep} \cdot (t-w)} \cdot dw \right) \cdot dt \quad (8)$$

where  $T$  is the radiation exposure time,  $t$  and  $w$  are integration time variables and  $D$ ,  $\dot{D}(t)$  and  $\mu_{rep}$  are the absorbed dose, dose rate at time  $t$  and the cell repair rate, respectively. Please note that the  $G$  factor does not intrinsically depend on the administered activity  $A_0$ , even though it depends on the absorbed dose (Eq. (6)) and on the dose rate (Eq. (5)). From Eq. (8), the constant value  $A_0$  in the two components of  $\dot{D}(t)$  (Eq. (5)) can be taken out of the integrals as  $A_0^2$  in the numerator. This cancels out with the  $A_0^2$  in the denominator produced by  $D^2$  (Eq. (6)).

For acute dose treatments (e.g. external-beam radiotherapy (EBRT)), the  $G$  factor is commonly assumed to be equal to 1. However, for prolonged dose treatments such as MRT, the  $G$  factor should be adequately computed for accurate SF calculations. Figure 6 illustrates the LQ model for an acute dose ( $G = 1$ ) with its respective components for lethal and sub-lethal damage.

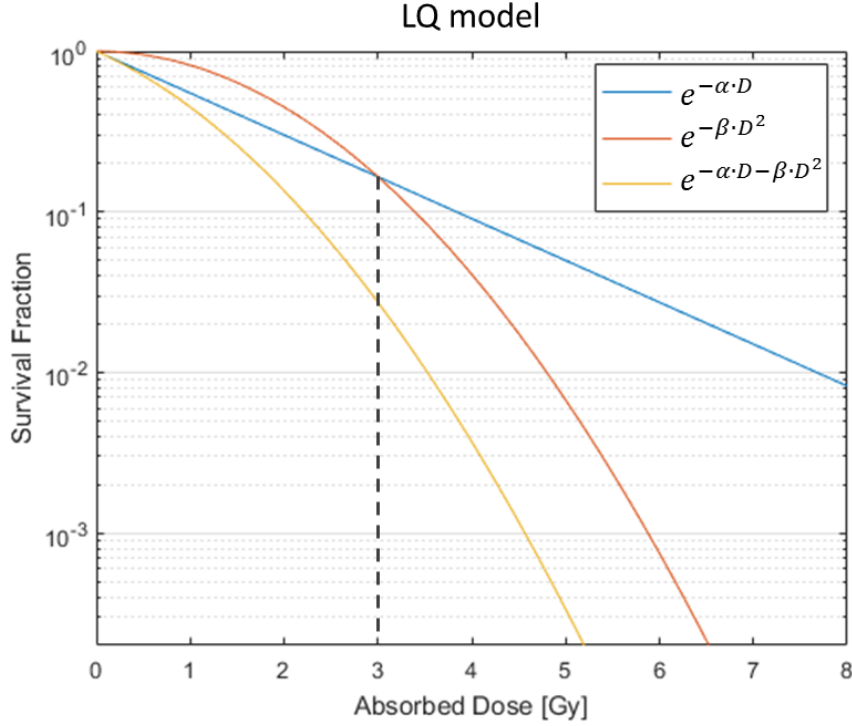


**Figure 6.** Representation of the linear-quadratic model. The lethal damage component (blue line) is proportional to the absorbed dose while the sub-lethal damage component (orange line) is proportional to the dose squared. The total biological effect (yellow line) considers both lethal and sub-lethal damage. The dashed black line divides the diagram in two regions: from 0 Gy to 3 Gy and higher than 3 Gy. In the first region, the lethal damage component prevails while in the second region the sub-lethal damage component produces the higher biological effect. This graph was created with values  $\alpha = 0.6 \text{ Gy}^{-1}$ ,  $\beta = 0.2 \text{ Gy}^{-2}$  ( $\alpha/\beta = 3 \text{ Gy}$ ) and  $G = 1$ .

Based on the LQ model, the BED (i.e. representation of dose accounting for the biological effect in a tissue) is defined as:

$$BED = D \cdot \left(1 + \frac{G}{\alpha/\beta} \cdot D\right) = -\frac{\text{Ln}(SF)}{\alpha} \quad (9)$$

where the ratio  $\alpha/\beta$  is commonly used to represent the sensitivity of a particular tissue to a particular type of ionising radiation (i.e. radiosensitivity). Although the values for  $\alpha$  and  $\beta$  should ideally be known to correctly describe the SF based on the absorbed dose using the LQ model, it is common to find in the literature only values for the ratio  $\alpha/\beta$  (in units of [Gy]) as the parameter representing the radiosensitivity of different tissues. Given Eq. (8), the same absorbed dose produces different BED values in tissues with different radiosensitivity [53]. Therefore, BED is usually presented in units of [ $Gy_{\alpha/\beta}$ ] (e.g. for a tissue with a ratio  $\alpha/\beta$  of 10 Gy, the BED is presented in units of [ $Gy_{10}$ ]).

BED values are mainly used to compare different radiation schemes (especially including fractionation (i.e. partition of the treatment in multiple fractions)) within a framework of isoeffective doses [53, 60]. However, because of the exponential



relationship between BED and SF (Eq. 9) (and therefore between BED and number surviving cells), comparisons and numerical operations (e.g. summation of radiation effects) using BED values are to be carefully and individually analysed.

Although absorbed doses are still more often used than BEDs for radiotherapy treatment planning and treatment evaluation, BED values have recently gained attention especially in MRT treatment assessment.

## **2.5 Treatment Planning in MRT**

Treatment planning in molecular radiotherapy comprises [7]:

- Selection of the appropriate radiopharmaceutical
- Determination of the activity to administer.
- Determination of the amount of pharmaceutical to administer.
- Evaluation of the use of additional pharmacokinetics-favouring substances.
- Determination of the administration schedule (i.e. the start and end of each administration).

The radionuclide and administration schedule to use are commonly defined based on the malignancy to treat and as a result of a clinical trial (or multiple clinical trials) in which the therapeutic effectiveness of the radiopharmaceutical and the side effects produced by the radiopharmaceutical under an specific administration schedule are considered [7]. Traditionally, treatment planning in MRT has been performed by only determining the activity to administer using a fixed administration schedule for a defined radiopharmaceutical without considering the pharmaceutical amount, which has been commonly neglected as a treatment-modulation factor [7, 62]. Thus, the pharmaceutical amount has routinely been determined by the specific/molar activity achieved in-situ during the radiopharmaceutical synthesis for the planned activity. The low relevance given to the pharmaceutical amount in MRT over the years is evidenced by the fact that only the administered activity (and not the pharmaceutical amount or the specific/molar activity) is reported in most MRT publications. However, it has been recently demonstrated that the pharmaceutical amount is an import treatment modulator as it changes the relative pharmacokinetics between the OARs and the target tissue (e.g. the tumour) allowing potential improvement of the therapeutic index [4, 17, 19]. Therefore, the pharmaceutical amount (and possibly the administration schedule) needs to be considered for adequate treatment planning in MRT [4].

The importance of using pharmacokinetics-favouring substances (unlabelled pharmaceutical or other nonradioactive substances, e.g. amino acids) for treatment planning in MRT has also been demonstrated [63, 64]. These kinds of substances are administered to exploit the pharmacokinetic differences between the OARs and the target tissue. For instance, some organs/tissues have a faster uptake of a nonradioactive substance than the tumour lesions. As such, an early acute load of

this nonradioactive substance can be used to saturate the OAR receptors before the radioactive administration hence reducing the OAR radiopharmaceutical uptake [63, 64]. Pharmacokinetics-favouring substances can be administered before (i.e. preload) or simultaneously with (i.e. co-infusion) the radiopharmaceutical. Infusions of pharmacokinetics-favouring substances starting before and continuing during the radiopharmaceutical administration are also used in practice (e.g. in PRRT, a 4-hour infusion of an amino acid solution is routinely administered 30 min before the start of the radiopharmaceutical infusion to reduce the radiopharmaceutical accumulation in the kidneys [35]). However, the application of pharmacokinetics-favouring substances may also reduce the accumulation of radiopharmaceutical in the target tissue, and therefore adequate planning is required before their administration.

Different methods for treatment planning are used in MRT, which vary in complexity, costs, level of individualisation and outcomes [7]. According to the level of individualisation, two main categories of treatment planning methods exist in MRT: cohort-based and patient-based [7].

In cohort-based treatment planning, the applied therapeutic plan (i.e. activity to administer, pharmaceutical amount and administration schedule) is determined by a previous study (e.g. a clinical trial) in which high standards of safety and efficacy are adopted [7]. In cohort-based studies, as in chemotherapy, the dosage (i.e. activity and/or pharmaceutical amount) to administer is determined by step-wise dosage escalation for a specific group of patients until reaching a mean incidence of a defined maximum tolerated toxicity [7, 62]. The dosage resulting from a cohort-based study can be further adapted based on patient characteristics such as body weight, disease stage or count of erythrocytes [7]. However, as there are inter-individual physiological differences and the patient-specific pharmacokinetics is not considered (low level of individualisation), the cohort-based approach can lead to under- and over-dosage [7, 16].

In contrast to the cohort-based approach, in patient-based treatment planning the patient-specific pharmacokinetics is considered to individually determine the treatment plan to use (higher level of individualisation) [7]. Typically, patient pretherapeutic quantitative data (e.g. series of PET images) for the same or a similar radiopharmaceutical or data from a previous MRT treatment are used to determine patient-specific pharmacokinetics [7, 62]. A basic approach of patient-specific treatment planning is dosimetry-based treatment planning (DBTP), in which individual dosimetric calculations for the main OARs and the target are considered to determine the activity to administer [62]. For some fractionated treatments (treatments with multiple fractions (i.e. cycles)), the dosimetry-based approach consists in delivering cycles with a fixed activity until a specified dose limit (absorbed dose or BED) for the OARs is reached [62, 65]. In DBTP only the activity to administer (and not the pharmaceutical amount or the administration schedule) can be included in the planning process. Thus, accurate results using DBTP may only be achieved when the pharmaceutical amounts and administration schedules for the planning

administration and the therapeutic administration are similar. A more sophisticated approach of patient-specific treatment planning is based on patient-specific pharmacokinetic parameters and pharmacokinetic models (e.g. PBPK models) [7]. A general description of the pharmacokinetic-model-based treatment planning approach is given in Figure 7 [7].

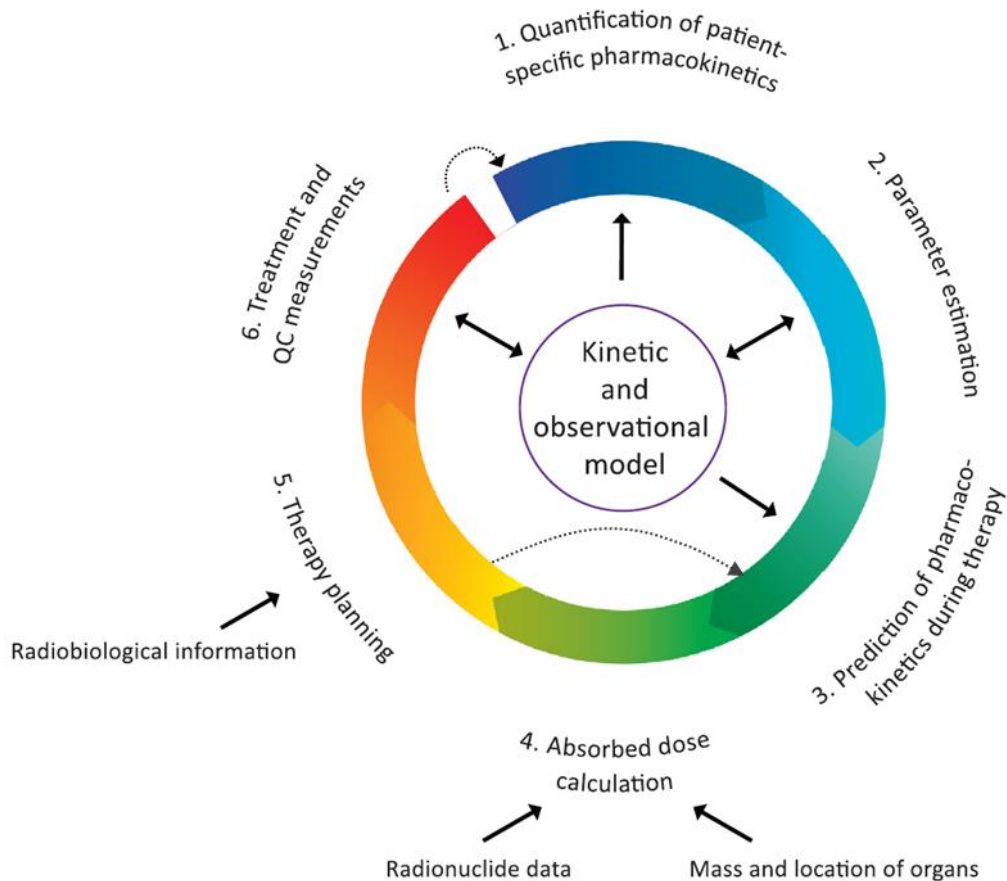


**Figure 7.** Algorithm for pharmacokinetic-model-based treatment planning in molecular radiotherapy (modified from Glatting et al. [7]).

MRT treatment planning based on individualised pharmacokinetic models (including PBPK models) consist in six well-defined steps [7]:

1. Quantification of patient-specific pharmacokinetics using pretherapeutic quantitative data. Quantitative data can be used to validate a pharmacokinetic model and/or to individually estimate unknown pharmacokinetic parameters.
2. Definition of individual pharmacokinetic parameters. These parameters can be measured, estimated or defined based on well-founded assumptions. Allometric scaling is commonly used to estimate unknown pharmacokinetic parameters. In addition, pharmacokinetic parameters can be estimated by fitting a validated pharmacokinetic model to individual quantitative data.

3. The individualised pharmacokinetic model is adapted to therapy conditions (e.g. by changing the nuclide half-life and/or the radiopharmaceutical amount) and simulations/estimations of pharmacokinetics for therapy are performed.
4. Absorbed doses for the OARs and target region are calculated using the simulated pharmacokinetics.
5. The treatment is planned based on the calculated absorbed doses and considering potential additional absorbed dose/BED restrictions for the OARs. Simulations of pharmacokinetics varying the treatment conditions (i.e. amount, activity and administration schedule) followed by new dose calculations are performed until optimal/acceptable characteristics for therapy (i.e. planned treatment) are achieved [4, 17, 18, 64].
6. The planned treatment is applied and additional measurements for quality control are performed. These measurements are used to verify treatment effectiveness and OAR toxicity and can also be utilised to improve the pharmacokinetic model for subsequent therapy cycles.

For each therapeutic cycle the full treatment planning algorithm (as described above) should be applied.

As treatment planning based on pharmacokinetic models uses a mechanistic approach, not only the activity but also the pharmaceutical amount, the administration schedule and the use of pharmacokinetics-favouring substances can potentially be planned depending on the used pharmacokinetic model [4, 64].

### 3 MATERIALS AND METHODS

In this chapter, the developed concepts of overall biologically effective dose (oBED) and overall tumour control probability (oTCP) are presented. The concept of virtual patients is also introduced and the characteristics of the virtual patients (including the description of the used PBPK model) considered in the conducted *in silico* clinical trial are given. The main part of this section is the description of the workflow of the developed treatment planning algorithm [66]. Lastly, the parameters used in the simulations performed in the *in silico* clinical trial are presented.

An overview of relevant abbreviations used in this section and their respective definitions are presented in Table I.

**Table I.** Relevant abbreviations for the developed treatment planning algorithm.

Abbreviation	Full form	Meaning
CLAAC	Combined limiting amount-activity curve	LAAC resulting from considering all the constraints for the organs at risk and for the radiopharmaceutical.
LAAC	Limiting amount-activity curve	Curve representing the maximum tolerated or achievable activity for each peptide molar amount. It can be based on an organ biologically effective dose constraint (maximum tolerated activity) or on a radiopharmaceutical constraint (maximum achievable activity).
MA	Molar activity	Ratio between activity [Bq] and peptide amount [mol].
oBED	Overall biologically effective dose	Biologically effective dose representing organs/tissues with inhomogeneous characteristics or distribution (e.g. multiple tumour lesions).
oSF	Overall survival fraction	Total survival fraction considering a group of tumour lesions.
oTCP	Overall tumour control probability	Probability of achieving tumour control considering a group of tumour lesions.

#### 3.1 Overall Biologically Effective Dose

The efficacy of a therapeutic plan in molecular radiotherapy or in any other cancer treatment depends on the number of killed/sterilised tumour cells. Nevertheless, it is common practice to determine the outcome of a radiotherapy treatment based on the tumour absorbed dose or BED for individual lesions. For patients with multiple tumour lesions, maximising the combined summation of the absorbed doses or BEDs in the lesions does not guarantee an optimal plan, unless all lesions have the same number of cells. This is because of the exponential relationship between the survival fraction

(SF) and the absorbed dose or BED and due to differences in the number of tumour cells between the lesions as shown in Eq. (10)

$$SF = \frac{Cells_s}{Cells_T} = e^{-BED \cdot \alpha} = e^{-\alpha \cdot D - G \cdot \beta \cdot D^2} \quad (10)$$

where SF is the survival fraction,  $Cells_s$  is the number of surviving cells,  $Cells_T$  is the total number of cells before irradiation,  $G$  is the Lea-Catcheside factor [60],  $D$  is the absorbed dose and  $\alpha$  and  $\beta$  are the linear and quadratic parameters of the linear-quadratic (LQ) model.

Based on Eqs. (9) and (10), the total number of surviving tumour cells after irradiation considering multiple lesions can be expressed as:

$$Cells_{s\_T} = \sum_{i=1}^N Cells_{s\_i} = \sum_{i=1}^N Cells_{T\_i} \cdot (e^{-\alpha_i \cdot BED_i}) \quad (11)$$

$$Cells_{s\_T} = \sum_{i=1}^N Cells_{T\_i} \cdot (e^{-\alpha_i \cdot D_i - G_i \cdot \beta_i \cdot D_i^2}) \quad (12)$$

where  $Cells_{s\_T}$  is the total number of surviving cells for all the considered lesions,  $N$  is the number of considered lesions,  $Cells_{s\_i}$  is the number of surviving cells for each considered lesion,  $Cells_{T\_i}$  is the initial number of tumour cells for each lesion,  $\alpha_i$  and  $\beta_i$  are the linear and quadratic parameters of the LQ model for each lesion and  $BED_i$ ,  $D_i$  and  $G_i$  are the BED, the absorbed dose and the Lea-Catcheside factor for each lesion, respectively.

Eqs. (11) and (12) can also be expressed in terms of the mass and the cell density of the considered tumour lesions as follows:

$$Cells_{s\_T} = \sum_{i=1}^N m_i \cdot \rho_i \cdot (e^{-\alpha_i \cdot BED_i}) \quad (13)$$

$$Cells_{s\_T} = \sum_{i=1}^N m_i \cdot \rho_i \cdot (e^{-\alpha_i \cdot D_i - G_i \cdot \beta_i \cdot D_i^2}) \quad (14)$$

where  $m_i$  and  $\rho_i$  are the mass and the cell density of each tumour lesion, respectively.

From Eqs. (13) and (14), the overall survival fraction (oSF) can be derived as:

$$oSF = \frac{Cells_{s\_T}}{Cells_T} = \frac{\sum_{i=1}^N m_i \cdot \rho_i \cdot (e^{-\alpha_i \cdot BED_i})}{\sum_{i=1}^N m_i \cdot \rho_i} \quad \text{with} \quad Cells_T = \sum_{i=1}^N Cells_i \quad (15)$$

$$oSF = \frac{Cells_{s\_T}}{Cells_T} = \frac{\sum_{i=1}^N m_i \cdot \rho_i \cdot (e^{-\alpha_i \cdot D_i - G_i \cdot \beta_i \cdot D_i^2})}{\sum_{i=1}^N m_i \cdot \rho_i} \quad (16)$$

where  $Cells_T$  is the total number of tumour cells among all the considered lesions.

Based on Eq. (9), oSF can be converted into an overall BED (oBED) as follows:

$$oBED = -\frac{\ln(oSF)}{\alpha} = -\frac{1}{\alpha} \cdot \ln \left( \frac{\sum_{i=1}^N m_i \cdot \rho_i \cdot (e^{-\alpha_i \cdot BED_i})}{\sum_{i=1}^N m_i \cdot \rho_i} \right) \quad (17)$$

$$oBED = -\frac{1}{\alpha} \cdot \ln \left( \frac{\sum_{i=1}^N m_i \cdot \rho_i \cdot (e^{-\alpha_i \cdot D_i - G_i \cdot \beta_i \cdot D_i^2})}{\sum_{i=1}^N m_i \cdot \rho_i} \right) \quad (18)$$

where  $\alpha$  is an overall linear parameter of the LQ model representing all the considered lesions. As presented in Eq. (18), the tumour oBED represents a BED accounting for the total surviving tumour cells (or clonogenic tumour cells) in the selected lesions. Note that for a single lesion the oBED is identical to the BED.

The value of  $\alpha$  in Eq. (18) is defined (Eq. (27)) such as the total number of surviving cells is equal when using the oBED with the overall  $\alpha$  value and when individual BEDs ( $BED_i$ ) and  $\alpha$  values ( $\alpha_i$ ) are considered for every lesion, as shown in Eq. (19):

$$Cells_{s\_T} = Cells_T \cdot (e^{-\alpha \cdot oBED}) = \sum_{i=1}^N Cells_{T\_i} \cdot (e^{-\alpha_i \cdot BED_i}) \quad (19)$$

As  $\alpha$  and  $oBED$  are interdependent in Eq. (19), a single  $\alpha$  value cannot be derived. To solve this interdependence, a first order Taylor expansion was used to make approximations of these expressions as presented from Eq. (20) to Eq. (26).

$$Cells_T \cdot (e^{-\alpha \cdot oBED}) \sim Cells_T \cdot (1 - \alpha \cdot oBED) \quad (20)$$

$$Cells_T \cdot (e^{-\alpha \cdot oBED}) \sim Cells_T - Cells_T \cdot \alpha \cdot oBED \quad (21)$$

$$\sum_{i=1}^N Cells_{T\_i} \cdot (e^{-\alpha_i \cdot BED_i}) \sim \sum_{i=1}^N Cells_{T\_i} \cdot (1 - \alpha_i \cdot BED_i) \quad (22)$$

$$\sum_{i=1}^N Cells_{T\_i} \cdot (e^{-\alpha_i \cdot BED_i}) \sim Cells_T - \sum_{i=1}^N Cells_{T\_i} \cdot \alpha_i \cdot BED_i \quad (23)$$

Then, Eq. (24) can be derived from Eq. (19), Eq. (21) and Eq. (23).

$$Cells_T \cdot \alpha \cdot oBED = \sum_{i=1}^N Cells_{T\_i} \cdot \alpha_i \cdot BED_i \quad (24)$$

In case that all  $BED_i = oBED$  and that for all lesions  $\alpha_i \cdot BED_i \ll 1$ , it follows:

$$Cells_T \cdot \alpha = \sum_{i=1}^N Cells_{T\_i} \cdot \alpha_i \quad (25)$$

$$\alpha = \frac{\sum_{i=1}^N Cells_{T\_i} \cdot \alpha_i}{Cells_T} \quad (26)$$

Considering the individual tumour masses and tumour cell densities, Eq. (26) can be written as:

$$\alpha = \frac{\sum_{i=1}^N m_i \cdot \rho_i \cdot \alpha_i}{\sum_{i=1}^N m_i \cdot \rho_i} \quad (27)$$

Assuming the same  $\alpha_i$  parameter ( $\alpha$ ),  $\beta_i$  parameter ( $\beta$ ) and tumour cell density ( $\rho$ ), Eq. (17) and Eq. (18) can be simplified to:

$$oBED = -\frac{1}{\alpha} \cdot \ln \left( \frac{\sum_{i=1}^N m_i \cdot (e^{-\alpha \cdot BED_i})}{\sum_{i=1}^N m_i} \right) \quad (28)$$

$$oBED = -\frac{1}{\alpha} \cdot \ln \left( \frac{\sum_{i=1}^N m_i \cdot (e^{-\alpha \cdot D_i - G_i \cdot \beta \cdot D_i^2})}{\sum_{i=1}^N m_i} \right) \quad (29)$$

Maximising the oBED as defined in this work leads to maximising the number of killed tumour cells among the considered tumour lesions.

### 3.2 Overall Tumour Control Probability

The relationship between radiation and cell survival is stochastic (i.e. described by a probabilistic model) [67]. Therefore, the effectiveness of a radiotherapy treatment is also stochastic. The probability of achieving an effective treatment of a tumour lesion is called tumour control probability (TCP) and depends on the number of surviving tumour clonogenic cells (i.e. cells able to proliferate). Therefore, TCP is commonly defined based on the survival fraction of the tumour clonogenic cells after radiotherapy treatment as follows [68]:

$$TCP = e^{-n_0 \cdot (SF)} \quad (30)$$

where  $n_0$  is the initial number of tumour clonogenic cells (i.e. clonogens) and SF is the survival fraction of the tumour clonogens after irradiation. Thus, for multiple tumour lesions and based on the developed concept of overall survival fraction (oSf), the overall tumour control probability (oTCP) can be defined as:

$$oTCP = e^{-n_0 \cdot (oSf)} \quad (31)$$

From Eq. (31), the oTCP for multiple cycles can be estimated as:

$$oTCP = e^{-n_0 \cdot \left( \prod_{c=1}^{N_c} oSF_c \right)} \quad (32)$$

where  $n_0$  is the initial number of tumour clonogenic cells,  $N_c$  is the number of cycles and  $oSF_c$  is the overall SF for a particular cycle  $c$ . Eq. (32) can be used under the assumptions that (1) there is no or negligible tumour repopulation between cycles, (2) the number of tumour clonogens is large, (3) cell survival is a rare occurrence and (4) cell death is stochastically independent of other cells [69].

If the oSF is assumed equal for all the cycles, Eq. (32) can be simplified to:

$$oTCP = e^{-n_0 \cdot (oSF_c^{N_c})} \quad (33)$$



Eq. (32) and Eq. (33) are valid for tumours with doubling times (i.e. time needed to double the tumour size) much longer than the typical time between treatment cycles. This is the case for NETs (doubling time between 2.3 years and 3.7 years [70]) and meningioma (doubling time of 4.5 years [71]), which are usually treated with PRRT (common time between cycles from 6 weeks to 16 weeks [72]).

Complete treatment plans (i.e. including all the planned cycles) aim at achieving probabilities of having less than 1 tumour clonogen ( $TCP < 37\%$ ). However, adequate tumour control can be only defined for treatments producing at least 90 % TCP [68], with some authors defining adequate tumour control only for TCP values higher than 99 % [73].

### 3.3 Virtual Patients

A virtual patient is a computationally implemented mathematical model used to simulate different scenarios for real patients [74]. In this work, a virtual patient was defined as a whole-body PBPK model fitted to individually measured  $^{111}\text{In}$ -DOTATATE data from a patient with metastasising neuroendocrine tumours (NETs) or meningioma. Nine virtual patients were created and used for the conducted *in silico* clinical trial. To perform simulations with  $^{177}\text{Lu}$ -DOTATATE, the virtual patients created for  $^{111}\text{In}$ -DOTATATE were adapted by changing the nuclide half-life in the PBPK model (67.3 h for  $^{111}\text{In}$  [75] and 159.5 h for  $^{177}\text{Lu}$  [76]). The same numbering was kept for the virtual patients and the measured patients (Table II) (e.g. the virtual patient VP1 was generated with measured data from patient P1).

#### 3.3.1 Patient Data

Datasets from nine patients (*men* = 6, *women* = 3, *age* =  $(52 \pm 22)$  years) with metastasising NETs (*n* = 5) or meningioma (*n* = 4) injected with  $^{111}\text{In}$ -DOTATATE were used to generate the virtual patients considered in the conducted *in silico* clinical trial. The patient datasets considered in this study were the same as used by Kletting et al. [4] (however, only the first cycle of each patient was considered here). Each patient dataset consisted of a planar whole-body scintigraphy series (anterior and posterior), a computerised tomography (CT) image, serum time-activity data and a measurement of the glomerular filtration rate (GFR) using  $^{51}\text{Cr}$ -EDTA.

To generate pretherapeutic data, an intravenous infusion ( $(51 \pm 8)$  min) of DOTATATE ( $(75 \pm 10)$  nmol) labelled with  $^{111}\text{In}$  ( $(140 \pm 14)$  MBq) was administered to the patients. To reduce the nonspecific uptake of  $^{111}\text{In}$ -DOTATATE in the kidneys, 1,000 ml of a 2.5 % solution of amino acids (lysine and arginine) was co-administered over 2 h, starting 0.5 h before the infusion of the radiopharmaceutical. Planar scintigraphy images taken with a e.cam® gamma camera (Siemens, Erlangen, Germany) were acquired 2 h, 4 h, 1 d, 2 d and 3 d after the end of the

peptide infusion. Blood samples were taken 5 min, 15 min, 30 min, 1 h, 2 h, 4 h, 1 d, 2 d and 3 d following the completion of the  $^{111}\text{In}$ -DOTATATE infusion. Activity concentrations in serum were measured using an Auto- $\gamma$ -5003 gamma counter (CANBERRA PACKARD Central Europe GmbH, Schwadorf, Austria). ULMDOS [77] and NUKDOS [78] software packages were used to retrieve time-activity data from the scintigraphy images for the liver, kidneys, spleen, tumour lesions and whole body. Two tumour lesions were considered in each patient except in patients 2, 4 and 5, for whom only one lesion was found. Activity data for the RM could not be directly retrieved. CT images were used to individually determine the volumes of the liver, kidneys, spleen and tumour lesions for each patient. Patient characteristics are shown in Table II.

**Table II.** Patient characteristics.

Patient	Tumour	Sex	Age (years)	BW (kg)	Tumour Volumes (ml)	
					Lesion 1	Lesion 2
P1	Men	M	31	78	87	20
P2	Men	M	31	81	116	-
P3	Men	F	56	84	2	0.5
P4	Men	M	70	86	3	-
P5	NET	M	76	78	2520 <sup>a</sup>	-
P6 <sup>b</sup>	NET	F	33	71	4	30
P7	NET	M	73	80	111	23
P8	NET	F	83	57	13	2
P9	NET	M	78	69	3	5

<sup>a</sup> Estimated tumour volume,  $V_{\text{TU}} = V_{\text{Liver\_Total}} - V_{\text{Liver\_Total\_Average}}$  where  $V_{\text{TU}}$  is the tumour volume,  $V_{\text{Liver\_Total}}$  is the measured liver volume and  $V_{\text{Liver\_Total\_Average}}$  is the average liver volume for a male of the same weight. This calculation was performed due to the very large size of the tumour.

<sup>b</sup> Patient with splenectomy.

Men, meningioma; NET, neuroendocrine tumour; BW, body weight.

### 3.3.2 PBPK Model

A  $^{111}\text{In}$ -DOTATATE whole-body PBPK model previously created and validated by Kletting et al. [4] was implemented and used as a basis for creating the nine virtual patients used to perform simulations of pharmacokinetics. This model individually considers peptide pharmacokinetics in the kidneys, liver, RM, spleen, gastrointestinal track, lungs, muscles, adrenal glands, prostate, bones, heart, brain, adipose tissue, skin, arteries, veins and in two tumour lesions. The rest of the organs and tissues are grouped as the remainder. The model incorporates physiological characteristics such as distribution, vascular permeability, specific binding, internalisation, degradation and excretion. Two parallel systems constitute the model: labelled and unlabelled peptide [79]. These systems are linked by the physical decay of the radionuclide and compete for the available targeted receptors in the organs in a nonlinear interaction

[79]. Substance transfer among the organs is determined by the organ vascular volumes and blood flows. A scheme of the used PBPK model is presented in Figure 5 (section 2.3).

The described model was implemented in SAAM II (version 2.2, The Epsilon Group, Washington, USA) [50], where individualised PBPK model parameters were determined for each patient by fitting the model parameters to the patient pharmacokinetic data allowing to create virtual patients for  $^{111}\text{In}$ -DOTATATE [4, 19]. The fitting process considered patient-specific measured or scaled anatomical and physiological data as well as measured  $^{111}\text{In}$ -DOTATATE pharmacokinetic data both of the respective patient and of other patients [4, 19].

The  $^{111}\text{In}$ -DOTATATE virtual patients were subsequently adapted to  $^{177}\text{Lu}$ -DOTATATE by changing the physical decay parameter (nuclide half-life of 67.3 h for  $^{111}\text{In}$  [75] and of 159.5 h for  $^{177}\text{Lu}$  [76]). The adapted  $^{177}\text{Lu}$ -DOTATATE virtual patients were implemented in Matlab/Simulink® to ease the automation of the simulation process. Model parameters for the virtual patients are the same as in Kletting et al. [4], being the nuclide half-life (159.5 h for  $^{177}\text{Lu}$ ) [76] the only changed parameter. The system of differential equations describing the used PBPK model was solved using SAAM II and the equations are described in the supplemental data in Kletting et al. [4].

$^{177}\text{Lu}$ -DOTATATE was selected for this *in silico* clinical trial because of the large amount of attention drawn to this substance over the last years. This radiopharmaceutical presents high affinity to the somatostatin receptor type 2 (sstr2) and has a maximal penetration depth of 1.7 mm, which permits a more localised treatment (i.e. less collateral damage) than with  $^{90}\text{Y}$ -labelled radiopharmaceuticals (maximum penetration depth of 11 mm) [3, 5]. Moreover,  $^{177}\text{Lu}$ -DOTATATE has shown high effectiveness and safety, producing lower toxicity in kidneys and RM than other therapeutic substances (e.g.  $^{90}\text{Y}$ -DOTATOC), and, in addition, allows post-therapy imaging [3, 5, 80].

### 3.4 Description of the Developed Treatment Planning Algorithm

The aim of treatment planning in molecular radiotherapy, after specifying the radiopharmaceutical and administration schedule to use, is to determine the combination of substance amount and activity yielding the maximum tumour cell sterilisation while avoiding high toxicity in the OARs [4, 7]. Thus, the maximum feasible tumour dose will be constrained by the maximum tolerated doses for the main OARs. The maximum achievable MA (proportional to the maximum achievable specific activity) of the radiopharmaceutical is an additional restriction for the achievable combinations of radiopharmaceutical amount and activity. Therefore, both dose constraints for the potentially dose-limiting organs and synthesis limitations of the radioactive drugs are to be considered in the treatment planning process in molecular radiotherapy.

Based on the work of Kletting et al. [4], a new treatment planning method to patient-specifically determine the optimal peptide amount and activity in PRRT was developed and implemented. This method, grounded on PBPK models, simultaneously considers the therapeutic effect in multiple tumour lesions, BED constraints for all the potentially dose-limiting organs and radiopharmaceutical synthesis limitations.

The workflow consists of two main phases:

1. An optimal activity (i.e. maximum activity) is calculated for each considered amount of radiopharmaceutical based on BED constraints for the potentially dose-limiting organs and on a radiopharmaceutical constraint (i.e. the maximum achievable MA).
2. The combination of amount and activity leading to the highest tumour oBED is selected as the optimal combination to administer.

Figure 8 illustrates the overall workflow of the developed treatment planning method.

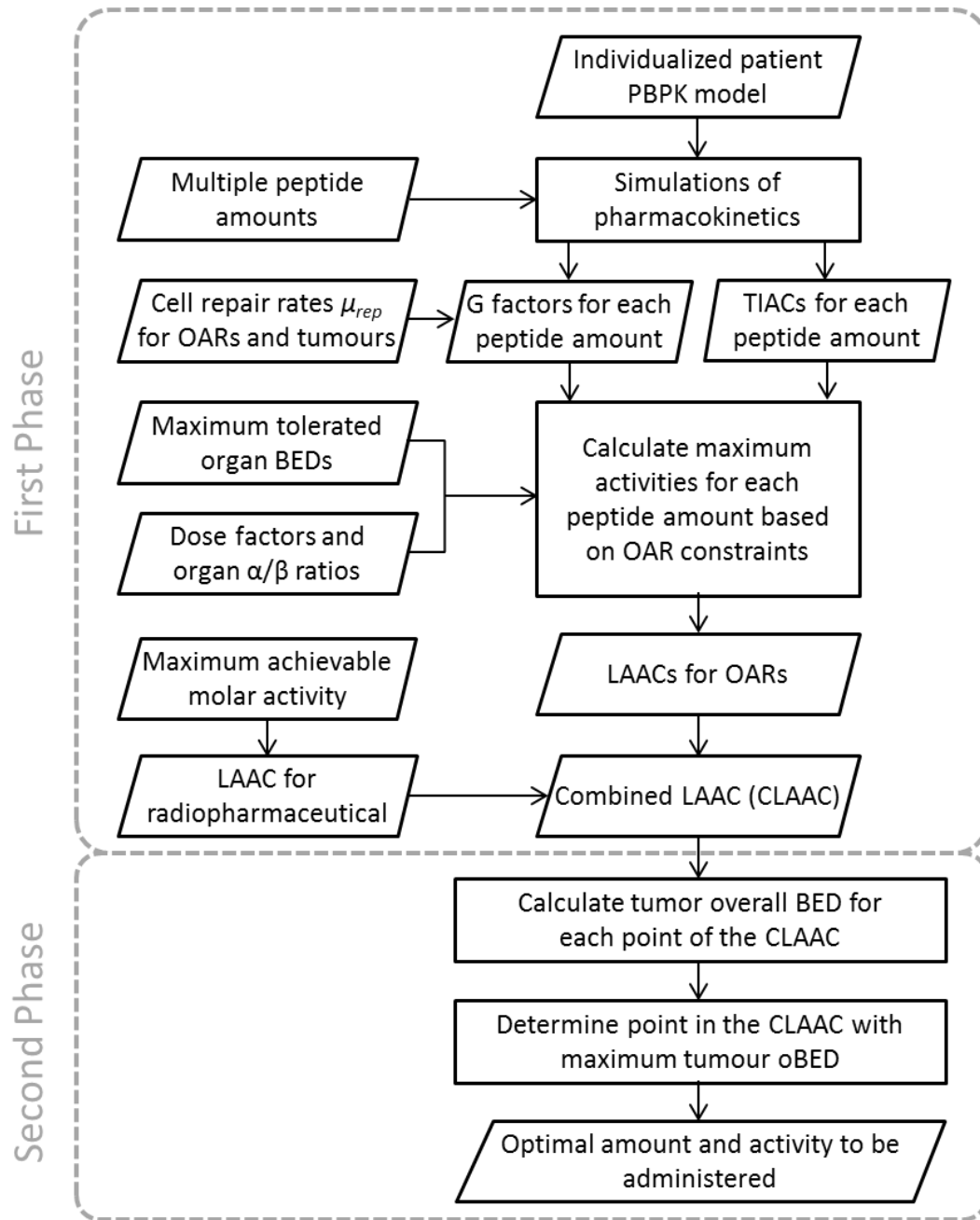


**Figure 8.** Workflow of the developed treatment planning algorithm. Tilted parallelograms represent inputs or outputs of a process while rectangles represent processes [81]. First, based on individual patient data a virtual patient is created to perform simulations of pharmacokinetics using different amounts of peptide. From the simulations of pharmacokinetics, time-integrated activity coefficients (TIACs) and G factors (Eq. (8)) are calculated for the OARs and tumour lesions. These parameters, together with the dose factors (also called S values), the OAR  $\alpha/\beta$  ratios and the specified maximum tolerated BEDs for the OARs are used to determine the maximum activities for each amount of peptide for each OAR (Eq. (37)). Maximum activities for each peptide amount are also calculated based on the maximum molar activity (MA) achievable during the radiopharmaceutical synthesis. Then, limiting amount-activity curves (LAACs) for each OAR and for the radiopharmaceutical are generated, with which the combined limiting amount-activity curve (CLAAC) is determined. The tumour overall BED (oBED) is calculated (Eq. (28)) for each point (amount, activity) in the CLAAC. The point on the CLAAC leading to the maximum tumour oBED is determined as the optimal amount and the optimal activity to administer to the respective patient.

First, a virtual patient is created based on the individual patient pharmacokinetic data and implemented in a program which supports numerical differentiation/integration and that, preferably, allows simulations varying the administered peptide amount in an automated way (e.g. Matlab/Simulink®). Maximum tolerated BEDs for each potentially dose-limiting OAR are determined. A maximum achievable radiopharmaceutical MA is also specified. Simulations are then performed for multiple peptide amounts within a range of interest, by preference using geometric step sizes (i.e. using a constant multiplication factor). For each simulated peptide amount, a maximum tolerated activity is calculated for each OAR. The equation used to calculate the maximum tolerated activity for a specific peptide amount for each OAR (Eq. (37)) is based on the maximum tolerated OAR BED and is derived from Eq. (6) and Eq. (9) as presented from Eq. (34) to Eq. (37):

Eq. (9) can be rewritten as:

$$\frac{G}{\alpha/\beta} \cdot D^2 + D - BED = 0 \quad (34)$$

Solving the quadratic equation for  $D$  in Eq. (34) results in:

$$D = \frac{-1 + \sqrt{1 + 4 \cdot \frac{G}{\alpha/\beta} \cdot BED}}{2 \cdot \frac{G}{\alpha/\beta}} \quad (35)$$

The second solution of the square root is not used for the further calculations as the absorbed dose cannot have negative values and  $G$  and  $\alpha/\beta$  are always positive values.

Inserting Eq. (6) in Eq. (35), assuming BED as the maximum tolerated OAR BED (and therefore representing the maximum tolerated OAR absorbed dose and the maximum tolerated administered activity  $A_{max}$ ) results in:

$$A_{max} \cdot \left( \sum_{rS=1}^N \tilde{a}_{rS}(T) \cdot S_{(rT \leftarrow rS)} \right) = \frac{-1 + \sqrt{1 + 4 \cdot \frac{G}{\alpha/\beta} \cdot BED_{max}}}{2 \cdot \frac{G}{\alpha/\beta}} \quad (36)$$

and after solving for  $A_{max}$  we obtain:

$$A_{max} = \frac{-1 + \sqrt{1 + 4 \cdot \frac{G}{\alpha/\beta} \cdot BED_{max}}}{2 \cdot \frac{G}{\alpha/\beta} \cdot \left( \sum_{rS=1}^N \tilde{a}_{rS}(T) \cdot S_{(rT \leftarrow rS)} \right)} \quad (37)$$

where  $A_{max}$  is the maximum tolerated activity for the OAR for a specific peptide amount,  $N$  is the number of organs/tissues considered in the dose calculations,  $\tilde{a}_{rS}(T)$  is the TIAC in each organ/tissue considered in the dose calculations for a

specific peptide amount,  $S_{(rT \leftarrow rS)}$  is the dose factor between each considered organ and the OAR,  $G$  is the Lea-Catcheside factor (which is independent from the administered activity) for the OAR for a specific peptide amount,  $\alpha$  and  $\beta$  are the linear and quadratic parameters of the LQ model for the OAR, and  $BED_{max}$  is the maximum tolerated OAR BED.

The calculated maximum tolerated activities for each amount define the limiting amount-activity curve (LAAC) for each OAR, such as every point in a LAAC represents an organ BED equal to its maximum tolerated dose (Figure 9). A LAAC is also generated for the radiopharmaceutical according to the maximum MA achievable during synthesis (Figure 9). Subsequently, a combined limiting amount-activity curve (CLAAC) is determined considering the minimum activity for each amount among all the LAACs (i.e. OARs plus radiopharmaceutical) (Figure 9). Thus, the CLAAC determines the maximum activity, and therefore the maximum tumour absorbed dose or BED, that can be administered for each peptide amount considering dose constraints for the OARs and limitations of the radiopharmaceutical synthesis. In addition, the region lying below the CLAAC represents all the achievable combinations of amount and activity accounting for the mentioned constraints (Figure 9).

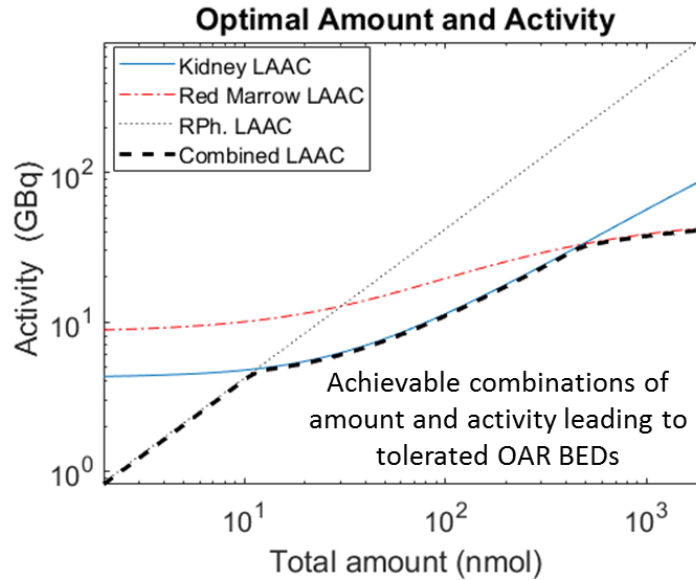


**Figure 9.** Limiting amount-activity curves. LAACs for kidneys (solid blue line), RM (dashed red line) and radiopharmaceutical (RPh.) (dotted black line) and definition of the CLAAC (bold dashed black line). The region of achievable combinations of amount and activity leading to tolerated OAR BEDs is below the CLAAC. This graph was produced by applying the described treatment planning algorithm to simulations for the virtual patient VP1. The maximum tolerated BEDs for the kidneys and RM were 10 Gy<sub>2.5</sub> and 0.5 Gy<sub>15</sub> per cycle, respectively. The maximum MA for <sup>177</sup>Lu-DOTATATE was determined by the highest practical MA reported in the literature that is 420 MBq/nmol [25].

To determine the optimal plan, tumour oBEDs are calculated (Eq. (17) or Eq. (28)) for each point (amount, activity) of the CLAAC. Considering tumour oBEDs instead of individual tumour BEDs allows to obtain a unique optimal plan for patients with multiple tumour lesions. Thereafter, the point in the CLAAC yielding the maximum tumour oBED (representing the maximum number of killed tumour cells among the considered lesions) is determined as the optimal amount and activity to administer to the patient for a respective cycle (Figure 10).

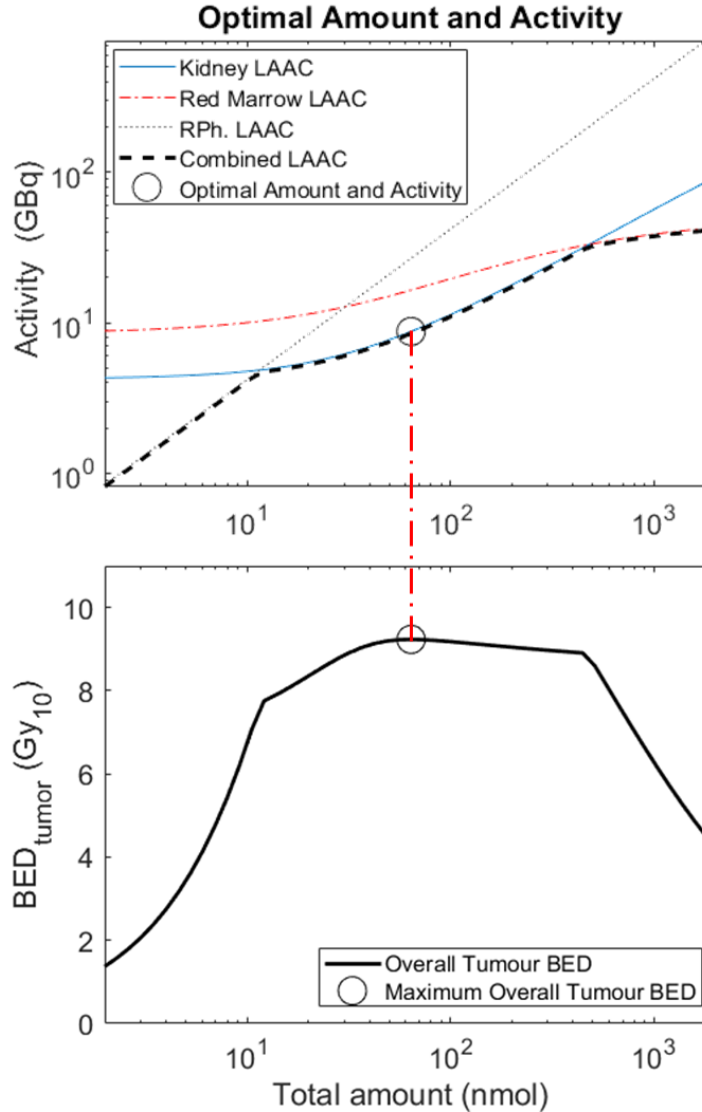


**Figure 10.** Determination of the optimal amount and activity. Top: definition of the CLAAC (bold dashed black line) and optimal point (amount, activity) in the CLAAC (circle); the abscissa axis corresponds to the total amount of substance and was not written to simplify the diagram. Bottom: tumour oBED curve (solid line) indicating the maximum tumour oBED accounting for the specified constraints (circle). The points of the tumour oBED curve were calculated with the combinations of amount and activity defined by the CLAAC. The dash-dot bold red line connecting the bottom and top diagrams links the maximum tumour oBED (bottom circle) with the combination of amount and activity which produces it (top circle). The graphs in this figure correspond to applying the described method to simulations for the virtual patient VP1. The same parameters as in Figure 9 were used.



### 3.5 *In Silico* Clinical Trial

The developed  $^{177}\text{Lu}$ -DOTATATE virtual patients were implemented in Matlab/Simulink® (MathWorks, Natick, Massachusetts, USA) to perform simulations of pharmacokinetics for different amounts of peptide. For each virtual patient, simulations were performed varying the peptide amount from 2 nmol to 2048 nmol in geometric step sizes of  $\sqrt[5]{2}$  (51 different amounts) for a fixed infusion time of 30 min [72, 82]. For each amount, 1000 h of therapy time ( $> 6$  half-lives of  $^{177}\text{Lu}$  [76]) were simulated using the Accelerator mode in Simulink®. Maximum cumulative tolerated BEDs for the kidneys ( $40 \text{ Gy}_{2.5}$  [83]) and for the RM ( $2 \text{ Gy}_{15}$  [4, 84]) were assumed. A total of 4 PRRT cycles were assumed for the completion of the treatment [3, 72, 80], leading to maximum tolerated BEDs per cycle of  $10 \text{ Gy}_{2.5}$  and  $0.5 \text{ Gy}_{15}$  for the kidneys and the RM, respectively. The highest practical MA reported in the literature for  $^{177}\text{Lu}$ -DOTATATE ( $420 \text{ MBq/nmol}$  [25]) was used as radiopharmaceutical synthesis constraint. To calculate the absorbed doses in the OARs, dose factors (also called S values) for  $^{177}\text{Lu}$  were extracted from OLINDA/EXM [44], while dose factors for the tumour lesions were estimated based on their masses [85] (Appendix A, Table A - I). For BED calculations,  $\alpha/\beta$  ratios of 2.5 Gy were assumed for kidneys, liver and spleen, and of 15 Gy and 10 Gy for the RM and the tumour lesions, respectively [4, 86, 87]. Moreover, repair rates  $\mu_{\text{rep}}$  of  $\ln(2)/2.8 \text{ h}^{-1}$  were used for the kidneys, liver and spleen [14], and of  $\ln(2)/1.0 \text{ h}^{-1}$  and  $\ln(2)/1.5 \text{ h}^{-1}$  for the RM [88] and the tumour lesions [89], respectively. An  $\alpha$  value of  $0.35 \text{ Gy}^{-1}$  was used for all tumour lesions [86] to calculate the oBED (Eq. (17)). Tumour lesions were assumed to have the same cellular density ( $\rho$ ) and radiosensitivity ( $\alpha$ ) (Eq. (17)).

The maximum activities accounting for the specified kidney and RM tolerated BEDs were calculated for each simulated amount using Eq. (37). The maximum achievable activity for each peptide amount was also determined for each virtual patient based on the radiopharmaceutical synthesis limitation. After simulating all the included amounts, the LAACs for the kidneys, RM and radiopharmaceutical were created and the CLAAC was defined for each virtual patient. The tumour oBED (Eq. (28)) was calculated for each combination of amount and activity defined in the CLAAC for each virtual patient. The maximum tumour oBED in the CLAAC determined the optimal amount and activity to administer to each virtual patient. BEDs (Eq. (9)) for the kidneys, RM, liver, spleen and individual tumour lesions were calculated for each virtual patient with the optimal amount and activity. Individual and overall SFs for the tumour lesions were also computed for the optimal plans.

For comparison purposes, simulations using the developed  $^{177}\text{Lu}$ -DOTATATE virtual patients were also performed for a *typically* administered combination of amount (265 nmol) and activity ( $7.4 \text{ GBq}$ ) per cycle [72, 90]. BED and SF calculations for the *typical* plan were carried out in the same manner as for the optimal plans. oTCP values (Eq. (33)) were also estimated for one, two, three and four cycles of treatment for the optimal and *typical* plans.

Complete treatment plans (i.e. including the four planned cycles of  $^{177}\text{Lu}$ -DOTATATE) leading to an oTCP equal to or higher than 99 % [73] were defined in this *in silico* clinical trial as plans producing adequate tumour control.

The simulation time of each completed treatment planning process was registered (processor: Intel® Core™ i7-4790 @ 3.60 GHz, RAM: 16 GB, 64 bits).

### **3.6 Data Analyses and Statistics**

Mean and standard deviation (SD) values are presented for descriptive statistics. Maximum, minimum and median values were calculated to present ranges and typical values.

The Rosenbrock method for stiff differential equations was used in the simulations with Simulink® to solve the PBPK model equations and to perform other integral/derivative calculations. Variable time steps not longer than 30 min and with a maximum calculation error of 0.1 % per step were set in the Simulink® solver for all the simulations.

## 4 RESULTS

The resulting optimal amounts and activities obtained by applying the developed treatment planning algorithm (section 3.5) to the created virtual patients for the defined constraints are shown in Table III.

**Table III.** Optimal amounts and activities and BEDs and absorbed doses for the OARs and tumour lesions for the optimal plans. Results were obtained using the nine created  $^{177}\text{Lu}$ -DOTATATE virtual patients and simulating injections of different peptide amounts.

Virtual patient (Tumour)	Amount [nmol]	Activity [GBq]	$\text{oBED}_{\text{TU}}$ [Gy] <sup>a</sup>	$\text{BED}_{\text{K}}$ [Gy <sub>2.5</sub> ] (D <sub>K</sub> [Gy]) <sup>b</sup>	$\text{BED}_{\text{RM}}$ [Gy <sub>15</sub> ] (D <sub>RM</sub> [Gy]) <sup>c</sup>	$\text{BED}_{\text{TU}_1}$ [Gy <sub>10</sub> ] (D <sub>TU_1</sub> [Gy])	$\text{BED}_{\text{TU}_2}$ [Gy <sub>10</sub> ] (D <sub>TU_2</sub> [Gy])
VP1 (M)	64.0	8.9	9.2	10.0 (8.9) <sup>b</sup>	0.27 (0.27)	12.6 (12.3)	5.3 (5.2)
VP2 (M)	97.0	12.1	17.6	10.0 (9.0) <sup>b</sup>	0.31 (0.31)	17.6 (17.0)	-
VP3 (M)	512.0	29.8	2.8	10.0 (9.0) <sup>b</sup>	0.49 (0.49)	2.2 (2.1)	18.9 (18.2)
VP4 (M)	48.5	10.0	18.4	10.0 (8.4) <sup>b</sup>	0.25 (0.25)	18.4 (17.5)	-
VP5 (N)	73.5	9.0	106.7	5.8 (5.2)	0.50 (0.50) <sup>c</sup>	106.7 (100.3)	-
VP6 (N) <sup>d</sup>	24.3	6.2	18.7	10.0 (8.6) <sup>b</sup>	0.25 (0.25)	12.6 (12.2)	33.7 (31.9)
VP7 (N)	73.5	16.4	33.6	9.9 (8.6)	0.50 (0.50) <sup>c</sup>	52.0 (50.3)	28.6 (28.1)
VP8 (N)	64.0	9.2	54.2	9.2 (8.3)	0.50 (0.50) <sup>c</sup>	53.8 (52.1)	106.8 (100.4)
VP9 (N)	97.0	7.0	6.0	10.0 (8.6) <sup>b</sup>	0.31 (0.31)	7.1 (7.0)	5.8 (5.7)
Median	73.5	9.2	18.4	10.0 (8.6)	0.31 (0.31)	17.6 (17.0)	23.8 (23.2)
Min.	24.3	6.2	2.8	5.8 (5.2)	0.25 (0.25)	2.2 (2.1)	5.3 (5.2)
Max.	512	29.8	106.7	10.0 (9.0)	0.50 (0.50)	106.7 (100.3)	106.8 (100.4)

<sup>a</sup> Calculated with  $\alpha = 0.35 \text{ Gy}^{-1}$ .

<sup>b</sup> Dose-limiting organ. Kidney BED = 10 Gy<sub>2.5</sub>.

<sup>c</sup> Dose-limiting organ. Red marrow BED = 0.5 Gy<sub>15</sub>.

<sup>d</sup> Splenectomy.

M, meningioma; N, neuroendocrine tumour; D, absorbed dose.

Subscripts K, RM, TU, TU\_1 and TU\_2 stand for kidneys, red marrow, tumour, tumour lesion 1 and tumour lesion 2, respectively.

As shown in Table III, the optimal amount and activity ranged from 48.5 nmol to 512.0 nmol (median 80.5 nmol) and from 8.9 GBq to 29.8 GBq (median 11.5 GBq) for virtual patients with meningioma, and from 24.3 nmol to 97.0 nmol (median 73.5 nmol) and from 6.2 GBq to 16.4 GBq (median 9.0 GBq) for virtual patients with NETs. The median molar activity was 139 MBq/nmol ranging from 58 MBq/nmol (VP3) to 257 MBq/nmol (VP6) (Appendix B, Table A - III). In all virtual patients with meningioma the kidneys were the dose-limiting organ while in 3 out of 5 virtual patients with NETs (VP5, VP7 and VP8) the optimal treatment reached the constraint

for the maximum RM BED. In none of the simulated cycles the specified maximum achievable radiopharmaceutical MA (420 MBq/nmol) was the dominant constraint.

From all the performed simulations, the BED for meningioma lesions ranged from 2.2 Gy<sub>10</sub> to 18.9 Gy<sub>10</sub> (median 15.1 Gy<sub>10</sub>) and from 5.8 Gy<sub>10</sub> to 106.8 Gy<sub>10</sub> (median 33.7 Gy<sub>10</sub>) for NET lesions. Tumour oBED values for the optimal plans varied between 2.8 Gy and 106.7 Gy ( $\alpha = 0.35 \text{ Gy}^{-1}$ ). The median liver and spleen BEDs were 1.8 Gy<sub>2.5</sub> (range 1.0 Gy<sub>2.5</sub> to 3.8 Gy<sub>2.5</sub>) and 15.5 Gy<sub>2.5</sub> (range 11.9 Gy<sub>2.5</sub> to 25.9 Gy<sub>2.5</sub>), respectively (Appendix, Table A - III).

The mean simulation time for applying the presented treatment planning method evaluating 51 potentially optimal amounts was  $(2.6 \pm 0.1)$  min.

Figure 11 shows the diagrams for determining the optimal amount and activity (left), and the BEDs for the tumour lesions calculated for every point of the CLAAC (right) for 2 representative virtual patients (VP1 and VP8). Values for the *typical* plan (stars) are also included in Figure 11.

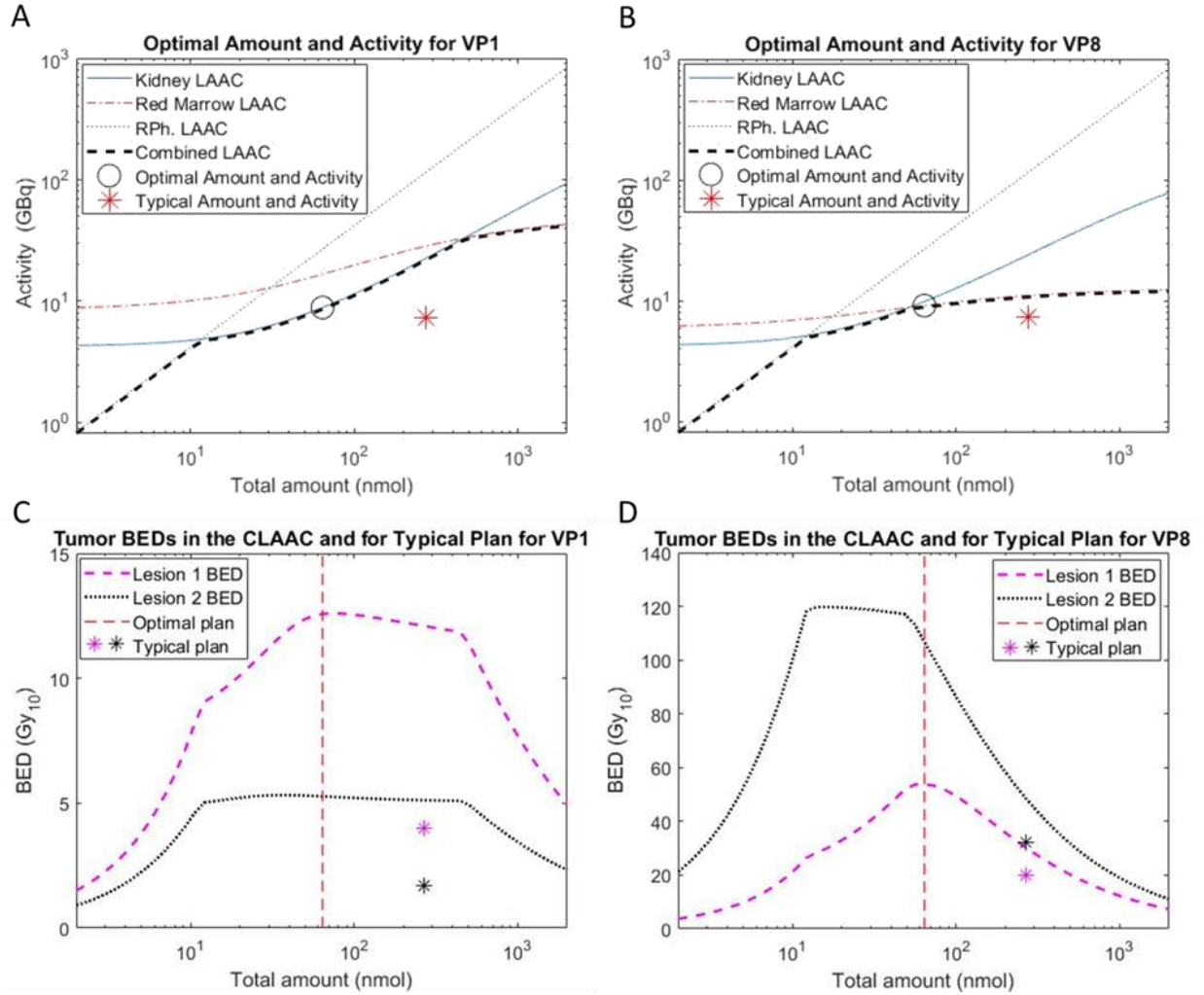


**Figure 11.** Optimal amount and activity and BEDs for the tumour lesions calculated for every point of the CLAAC for two representative virtual patients (Left: VP1; Right: VP8). Top: graphs illustrating the developed treatment planning algorithm plus the *typically* administered amount and activity (red star) [72, 90]. For VP1 (meningioma) the treatment is limited by the maximum tolerated kidney BED while for VP8 (NET) the dose-limiting organ is the RM. Bottom: BED vs peptide amount curves for the tumour lesions calculated for every point of the CLAAC. The vertical red dashed line represents the optimal amount, which intercepts the tumour BED curves at the BED values for the tumour lesions 1 and 2 when the optimal plan is applied. The magenta and black stars represent the BED for the tumour lesions 1 and 2 for the *typical* plan, respectively. Tumour lesion masses were 87 g (lesion 1) and 20 g (lesion 2) for VP1, and 13 g (lesion 1) and 2 g (lesion 2) for VP8. Note that the tumour lesion with larger mass has a higher influence on determining the optimal plan.

As shown in Figure 11 (top), the radiopharmaceutical synthesis determines the maximum activity (and therefore absorbed doses) for low peptide amounts; for intermediate amounts the kidneys are the dose-limiting organ, and for larger peptide amounts the RM is which limits the treatment. This same tendency was observed among all the virtual patients (graphs shown in Jiménez-Franco et al., supplement C [66]). What varied from virtual patient to virtual patient was the range of peptide amounts in which each of the constraints prevailed (for VP5 the kidneys did not limit

the treatment for any of the evaluated amounts). In addition, simulations of the *typically* delivered plan [72, 90] yielded results within the defined constraints for all the virtual patients (Table IV). The *typical* plan also produced considerably lower tumour BEDs than the optimal plans for the considered tumour lesions (Table III and Table IV).

The results of a simulated cycle for the *typically* delivered plan (265 nmol, 7.4 GBq, 30 min infusion) [72, 90] for the nine virtual patients are presented in Table IV.

**Table IV.** BEDs and absorbed doses for the OARs and tumour lesions resulting from simulating the *typically* administered amount (265 nmol) and activity (7.4 GBq) (MA = 28 MBq/nmol) [72, 90] for the created  $^{177}\text{Lu}$ -DOTATATE virtual patients.

Virtual Patient (Tumour)	$\text{oBED}_{\text{TU}}$ [Gy] <sup>a</sup>	$\text{BED}_{\text{K}}$ [Gy <sub>2.5</sub> ] (D <sub>K</sub> [Gy])	$\text{BED}_{\text{RM}}$ [Gy <sub>15</sub> ] (D <sub>RM</sub> [Gy])	$\text{BED}_{\text{TU}_1}$ [Gy <sub>10</sub> ] (D <sub>TU_1</sub> [Gy])	$\text{BED}_{\text{TU}_2}$ [Gy <sub>10</sub> ] (D <sub>TU_2</sub> [Gy])
VP1 (M)	3.4	3.1 (3.0)	0.13 (0.13)	4.0 (4.0)	1.7 (1.7)
VP2 (M)	5.3	3.0 (2.9)	0.14 (0.14)	5.3 (5.3)	-
VP3 (M)	1.4	3.7 (3.6)	0.15 (0.15)	0.8 (0.8)	7.5 (7.4)
VP4 (M)	4.7	2.5 (2.4)	0.11 (0.11)	4.7 (4.6)	-
VP5 (N)	65.4	3.3 (3.1)	0.39 (0.39)	65.4 (62.9)	-
VP6 (N) <sup>b</sup>	8.1	2.9 (2.8)	0.14 (0.14)	3.7 (3.7)	9.9 (9.8)
VP7 (N)	9.2	1.9 (1.9)	0.19 (0.19)	10.6 (10.6)	6.1 (6.0)
VP8 (N)	20.6	2.9 (2.8)	0.33 (0.33)	20.2 (19.9)	32.3 (31.7)
VP9 (N)	3.4	5.4 (5.0)	0.27 (0.27)	4.0 (4.0)	3.3 (3.3)
Median	5.3	3.0 (2.9)	0.15 (0.15)	4.7 (4.6)	6.8 (6.7)
Min.	1.4	1.9 (1.9)	0.11 (0.11)	0.8 (0.8)	1.7 (1.7)
Max.	65.4	5.4 (5.0)	0.39 (0.39)	65.4 (62.9)	32.3 (31.7)

<sup>a</sup> Calculated with  $\alpha = 0.35 \text{ Gy}^{-1}$ .

<sup>b</sup> Splenectomy.

M, meningioma; N, neuroendocrine tumour; D = absorbed dose.

Subscripts K, RM, TU, TU\_1 and TU\_2 stand for kidneys, red marrow, tumour, tumour lesion 1 and tumour lesion 2, respectively.

The simulations of a typical plan yielded tumour BEDs from 0.8 Gy<sub>10</sub> to 65.4 Gy<sub>10</sub> (median 5.3 Gy<sub>10</sub>) while the median BEDs for the kidneys and the RM were 3.0 Gy<sub>2.5</sub> (range 1.9 Gy<sub>2.5</sub> to 5.4 Gy<sub>2.5</sub>) and 0.15 Gy<sub>15</sub> (range 0.11 Gy<sub>15</sub> to 0.39 Gy<sub>15</sub>), respectively. Tumour oBED values ( $\alpha = 0.35 \text{ Gy}^{-1}$ ) ranged from 1.4 Gy to 65.4 Gy with a median of 5.3 Gy.

To compare the effectiveness of the optimal and the *typically* delivered plans, the tumour overall survival fractions (oSFs) (Eq. (15)) (as a representation of the total tumour cell killing/sterilisation) were calculated for each virtual patient after one, two, three and four PRRT cycles with  $^{177}\text{Lu}$ -DOTATATE (Table V). The total survival

fraction  $oSF_T$  after multiple cycles assuming the same survival fraction for each cycle can be calculated as:

$$oSF_T = oSF_c^{N_c} \quad (38)$$

where  $oSF_c$  is the overall SF for a particular cycle (the first cycle in this work) and  $N_c$  is the number of cycles.

**Table V.** Progression of the oSF through the cycles (for a total treatment of 4 cycles) for the typical and optimal plans with  $^{177}\text{Lu}$ -DOTATATE. The oSFs for all the cycles were assumed equal to the oSF for the first cycle for the nine virtual patients.

Virtual patient	oSF after 1 cycle		oSF after 2 cycles		oSF after 3 cycles		oSF after 4 cycles	
	Typical	Optimal	Typical	Optimal	Typical	Optimal	Typical	Optimal
VP1	$3.0 \times 10^{-1}$	$3.9 \times 10^{-2}$	$9.1 \times 10^{-2}$	$1.6 \times 10^{-3}$	$2.8 \times 10^{-2}$	$6.2 \times 10^{-5}$	$8.3 \times 10^{-3}$	$2.4 \times 10^{-6}$
VP2	$1.6 \times 10^{-1}$	$2.1 \times 10^{-3}$	$2.4 \times 10^{-2}$	$4.5 \times 10^{-6}$	$3.7 \times 10^{-3}$	$9.4 \times 10^{-9}$	$5.8 \times 10^{-4}$	$2.0 \times 10^{-11}$
VP3	$6.1 \times 10^{-1}$	$3.8 \times 10^{-1}$	$3.8 \times 10^{-1}$	$1.4 \times 10^{-1}$	$2.3 \times 10^{-1}$	$5.3 \times 10^{-2}$	$1.4 \times 10^{-1}$	$2.0 \times 10^{-2}$
VP4	$1.9 \times 10^{-1}$	$1.6 \times 10^{-3}$	$3.7 \times 10^{-2}$	$2.6 \times 10^{-6}$	$7.1 \times 10^{-3}$	$4.2 \times 10^{-9}$	$1.4 \times 10^{-3}$	$6.8 \times 10^{-12}$
VP5	$1.2 \times 10^{-10}$	$6.0 \times 10^{-17}$	$1.3 \times 10^{-20}$	$3.6 \times 10^{-33}$	$1.6 \times 10^{-30}$	$2.2 \times 10^{-49}$	$1.8 \times 10^{-40}$	$1.3 \times 10^{-65}$
VP6	$6.0 \times 10^{-2}$	$1.4 \times 10^{-3}$	$3.6 \times 10^{-3}$	$2.1 \times 10^{-6}$	$2.1 \times 10^{-4}$	$3.0 \times 10^{-9}$	$1.3 \times 10^{-5}$	$4.3 \times 10^{-12}$
VP7	$4.1 \times 10^{-2}$	$7.8 \times 10^{-6}$	$1.6 \times 10^{-3}$	$6.1 \times 10^{-11}$	$6.7 \times 10^{-5}$	$4.7 \times 10^{-16}$	$2.7 \times 10^{-6}$	$3.7 \times 10^{-21}$
VP8	$7.4 \times 10^{-4}$	$5.7 \times 10^{-9}$	$5.5 \times 10^{-7}$	$3.3 \times 10^{-17}$	$4.1 \times 10^{-10}$	$1.9 \times 10^{-25}$	$3.1 \times 10^{-13}$	$1.1 \times 10^{-33}$
VP9	$3.1 \times 10^{-1}$	$1.2 \times 10^{-1}$	$9.4 \times 10^{-2}$	$1.5 \times 10^{-2}$	$2.9 \times 10^{-2}$	$1.9 \times 10^{-3}$	$8.8 \times 10^{-3}$	$2.4 \times 10^{-4}$
Median	$1.6 \times 10^{-1}$	$1.6 \times 10^{-3}$	$2.4 \times 10^{-2}$	$2.6 \times 10^{-6}$	$3.7 \times 10^{-3}$	$4.2 \times 10^{-9}$	$5.8 \times 10^{-4}$	$6.8 \times 10^{-12}$
Min.	$1.2 \times 10^{-10}$	$6.0 \times 10^{-17}$	$1.3 \times 10^{-20}$	$3.6 \times 10^{-33}$	$1.6 \times 10^{-30}$	$2.2 \times 10^{-49}$	$1.8 \times 10^{-40}$	$1.3 \times 10^{-65}$
Max.	$6.1 \times 10^{-1}$	$3.8 \times 10^{-1}$	$3.8 \times 10^{-1}$	$1.4 \times 10^{-1}$	$2.3 \times 10^{-1}$	$5.3 \times 10^{-2}$	$1.4 \times 10^{-1}$	$2.0 \times 10^{-2}$

The comparison between the simulated optimal and typically delivered plans (Table V) shows that the optimal plans produced up to 6 orders of magnitude (VP5) smaller tumour oSFs (higher effectiveness at sterilising tumour cells) than the typical plan for the first cycle (24 orders of magnitude after 4 cycles). The tumour oSFs for the first  $^{177}\text{Lu}$ -DOTATATE cycles for the optimal and the typical plans ranged from  $6.0 \times 10^{-17}$  (VP5) to  $3.8 \times 10^{-1}$  (VP3) (median  $1.6 \times 10^{-3}$ ) and from  $1.2 \times 10^{-10}$  (VP5) to  $6.1 \times 10^{-1}$  (VP3) (median  $1.6 \times 10^{-1}$ ), respectively.

Assuming a tumour clonogenic cell density of  $1.12 \times 10^5$  cells/g [91] and based on the calculated oSFs for a single cycle (Table V), overall tumour control probability (oTCP) values were estimated (Eq. (33)) after one, two, three and four cycles of treatment (Table VI).

**Table VI.** Progression of the oTCP through the cycles (for a total treatment of 4 cycles) for the typical and optimal plans with  $^{177}\text{Lu}$ -DOTATATE. The oSFs for all the cycles were assumed equal to the oSF for the first cycle. The total tumour mass is the summation of the masses of all the considered tumour lesions in each virtual patient.

Virtual patient (Total tumour mass)	oTCP after 1 cycle		oTCP after 2 cycles		oTCP after 3 cycles		oTCP after 4 cycles	
	Typical	Optimal	Typical	Optimal	Typical	Optimal	Typical	Optimal
VP1 (107g)	0.00 <sup>a</sup>	0.00 <sup>a</sup>	0.00 <sup>a</sup>	0.00 <sup>a</sup>	0.00 <sup>a</sup>	0.00 <sup>a</sup>	0.00 <sup>a</sup>	$2.17 \times 10^{-13}$
VP2 (116 g)	0.00 <sup>a</sup>	0.00 <sup>a</sup>	0.00 <sup>a</sup>	$7.56 \times 10^{-26}$	0.00 <sup>a</sup>	$8.85 \times 10^{-1}$	0.00 <sup>a</sup>	1.00 <sup>b</sup>
VP3 (2.5 g)	0.00 <sup>a</sup>	0.00 <sup>a</sup>	0.00 <sup>a</sup>	0.00 <sup>a</sup>	0.00 <sup>a</sup>	0.00 <sup>a</sup>	0.00 <sup>a</sup>	0.00 <sup>a</sup>
VP4 (3 g)	0.00 <sup>a</sup>	0.00 <sup>a</sup>	0.00 <sup>a</sup>	$4.16 \times 10^{-1}$	0.00 <sup>a</sup>	$9.99 \times 10^{-1}$	0.00 <sup>a</sup>	1.00 <sup>b</sup>
VP5 (2520 g)	$9.68 \times 10^{-1}$	1.00 <sup>b</sup>	1.00 <sup>b</sup>	1.00 <sup>b</sup>	1.00 <sup>b</sup>	1.00 <sup>b</sup>	1.00 <sup>b</sup>	1.00 <sup>b</sup>
VP6 (34 g)	0.00 <sup>a</sup>	0.00 <sup>a</sup>	0.00 <sup>a</sup>	$3.81 \times 10^{-4}$	0.00 <sup>a</sup>	$9.89 \times 10^{-1}$	$8.21 \times 10^{-22}$	1.00 <sup>b</sup>
VP7 (134 g)	0.00 <sup>a</sup>	$1.71 \times 10^{-51}$	0.00 <sup>a</sup>	$9.99 \times 10^{-1}$	0.00 <sup>a</sup>	1.00 <sup>b</sup>	$2.36 \times 10^{-18}$	1.00 <sup>b</sup>
VP8 (15 g)	0.00 <sup>a</sup>	$9.90 \times 10^{-1}$	$3.94 \times 10^{-1}$	1.00 <sup>b</sup>	$9.99 \times 10^{-1}$	1.00 <sup>b</sup>	1.00 <sup>b</sup>	1.00 <sup>b</sup>
VP9 (18 g)	0.00 <sup>a</sup>	0.00 <sup>a</sup>	0.00 <sup>a</sup>	0.00 <sup>a</sup>	0.00 <sup>a</sup>	0.00 <sup>a</sup>	0.00 <sup>a</sup>	0.00 <sup>a</sup>

<sup>a</sup> Values smaller than or equal to  $1.0 \times 10^{-100}$

<sup>b</sup> Values larger than or equal to  $9.995 \times 10^{-1}$

According to the estimated oTCP values (Table VI), applying the optimal plans allows adequate tumour control (oTCP higher or equal to 99 %) in 6 out of the 9 virtual patients after 4 cycles of  $^{177}\text{Lu}$ -DOTATATE are administered. However, based on the results of the simulations, only in 2 virtual patients adequate tumour control was achieved after 4 cycles of the *typical* plan.

BED results for the liver and the spleen after the first cycle of  $^{177}\text{Lu}$ -DOTATATE for the optimal and typical plans are presented in Table A - III (Appendix B).



## 5 DISCUSSION

In this work an algorithm for individualised treatment planning in PRRT was presented and applied to simulations of pharmacokinetics with  $^{177}\text{Lu}$ -DOTATATE using nine virtual patients. To demonstrate the applicability and advantages of the developed algorithm, comparison was drawn between the optimal plans and the *typically* delivered plan using the same virtual patients.

Although the algorithm presented by Kletting et al. [4] was a first step towards individualised treatment planning in molecular radiotherapy, the algorithm was not suitable for clinical practice. To achieve clinical applicability, the algorithm presented in this work includes the following required enhancements and extensions:

1. Consideration of multiple potentially dose-limiting organs (e.g. kidneys and RM) in the optimisation process.
2. Incorporation of a radiopharmaceutical constraint (i.e. maximum achievable specific activity [MBq/ $\mu\text{g}$ ] or molar activity [MBq/nmol]).
3. Simultaneous consideration of all tumour lesions/metastases in the optimisation process by applying the developed concept of oBED.

Incorporating these features allows to derive a unique optimal plan (i.e. optimal peptide amount and activity to be administered) which maximises the total number of killed tumour cells in the considered lesions. Moreover, these improvements enable to consider every OAR as a potentially dose-limiting organ and to ensure that the resulting optimal amounts and activities can actually be administered to the patients in a safe way. Thus, the developed algorithm is general, effective, flexible and a relevant clinically applicable approach.

The presented algorithm uses the derived general equation for the oBED (Eq. (17)) to simultaneously consider multiple tumour lesions. This equation is a generalisation of the concept of equivalent uniform biologically effective dose (EUBED) presented by O'Donoghue [92] and by Cremonesi et al. [93]. The main difference between oBED (Eq. (17)) and EUBED is that Eq. (17) individually considers the radiation sensitivity ( $\alpha_i$ ) and the cell density ( $d_i$ ) for each lesion. This allows to individually include specific tumour characteristics (e.g. tumour stage or tumour oxygen enhancement ratio) in calculations or in treatment planning. Other authors have previously used the term “overall biologically effective dose (OBED)” [94]. However, the definition of the concept greatly differs from the equation developed in this work as it was defined as an algebraic summation of BED values [94].

The concept of oBED can also be used to calculate the cumulated tumour BED after multiple PRRT cycles considering tumour changes between cycles (e.g. changes in tumour mass [95]). Moreover, Eq. (17) can be applied to estimate the total BED for distributed organs such as the RM.

The main limitation of the introduced concept of oBED (Eq. (17)) is the need for  $\alpha_i$  values, which are not commonly found in the literature, where  $\alpha_i/\beta_i$  ratios are more frequently (but still rarely) given. An additional limitation of the oBED is that the general  $\alpha$  value representing all the considered lesions (Eq. (27)) may pose a challenge to compare doses from different plans or studies, especially for tumour lesions with different  $\alpha_i$  values. Therefore, comparison of treatments based on parameters such as the tumour control probability or the number of killed clonogenic tumour cells (or survival fraction) may lead to a broader consensus.

A more general form of Eq. (17) could also be formulated using single or multiple integrals to account for inhomogeneous uptake, inhomogeneous cell density and/or a changing radiation sensitivity [96-99]. However, this is beyond the scope of this work.

The results obtained for the *typical* plan with  $^{177}\text{Lu}$ -DOTATATE (Table IV) are in line with BED and absorbed dose values presented in the literature [65, 100, 101]. For the kidneys, more commonly performed dose calculations in PRRT, Sandström et al. obtained BED values (for the *typical* plan) ranging from 1.7 Gy<sub>2.6</sub> to 11.6 Gy<sub>2.6</sub> while the absorbed dose values ranged from 1.7 Gy to 9.8 Gy (right kidney) [100]. Sundlöv et al. obtained BED values from 2.3 Gy<sub>2.5</sub> to 19.1 Gy<sub>2.5</sub> and absorbed doses from 2.2 Gy to 14.3 Gy [65]. For the red marrow, Sandström et al. obtained absorbed doses from 0.05 to 0.4 Gy for the typical plan but did not perform BED calculations (red marrow BED values are expected to be very close to the absorbed doses because of the low dose values and the high  $\alpha/\beta$  value) [101]. These results are also in line with the results presented in Table IV.

The highly variable patient-specific optimal amounts (from 24.3 nmol to 512.0 nmol) and activities (from 6.2 GBq to 29.8 GBq) obtained in the conducted *in silico* clinical trial show the necessity of considering individual pharmacokinetics in treatment planning in MRT (e.g. using PBPK models). Individualised treatment planning may allow to safely increase the administered activity within controlled ranges of toxicity for the OARs while producing a higher tumour control [7], as shown in Table VI. Furthermore, Table VI shows that the *typical* plan may be insufficient to produce adequate tumour control after a 4-cycle treatment with  $^{177}\text{Lu}$ -DOTATATE while the optimal plans may produce adequate tumour control for most patients (6 out of 9 virtual patients).

As shown in Table III, the developed optimisation algorithm leads, in general, to lower peptide amounts and higher activities than the *typically* applied  $^{177}\text{Lu}$ -DOTATATE cycle. This implies a need for using higher molar activities than those routinely used to obtain more effective  $^{177}\text{Lu}$ -DOTATATE PRRT treatments. In addition, the fact that both the kidneys and the RM were the dose-limiting organs for different virtual patients indicates that these two organs need to be considered in treatment planning for PRRT. This also confirms the importance of performing accurate dosimetry for these organs [45, 102].

In the conducted *in silico* clinical trial, the assumed radiopharmaceutical constraint for  $^{177}\text{Lu}$ -DOTATATE (420 MBq/nmol) was never the dominant constraint in the treatment planning process when using the developed algorithm. However, this molar activity is the highest reported in the literature for  $^{177}\text{Lu}$ -DOTATATE [25]. Thus, considerably lower molar activities are routinely achieved for  $^{177}\text{Lu}$ -DOTATATE (e.g. 60 MBq/nmol [103], 38 MBq/nmol [104] and 28 MBq/nmol [72, 90]). Therefore, assuming a routinely achieved molar activity (or any other maximum achievable molar activity lower than 420 MBq/nmol) in the optimisation process will change the derived optimal plans. This will be explored in future work.

The median liver and spleen BED values obtained with the optimal plans are approximately triple the median BED values for these organs when the *typical* plan is applied (Appendix B, Table A – III). However, the median tumour BED value for the optimal plans are approximately quadruple the tumour BEDs produced by the *typical* plan (Table III and Table IV). This leads in general to achieve higher therapeutic indices considering these organs when the optimal plans are delivered. The considerably higher BED values for the liver and the spleen for the optimal plans may indicate that these organs need to be included as potentially dose-limiting organs in the treatment planning algorithm (maximum tolerated BED values need to be determined).

Comparison between the tumour BEDs for the optimal and *typically* delivered plans could be drawn from Table III and Table IV. However, BED differences should be carefully and individually analysed because of the nonlinear relationship between the BED and the survival fraction. Therefore, comparison of the tumour BED values was not performed in this work.

Applying the developed algorithm may also result in economic benefits represented in less peptide amount per patient and less number of cycles because of the increased tumour sterilisation.

The presented treatment planning algorithm can also be used for other therapies using radiolabeled ligands (e.g. radioimmunotherapy) [4, 17-19, 105]. Moreover, as the algorithm is based on PBPK model, it can additionally include the optimisation of the administration schedule which may also consider the use of additional substances for modulation of individual pharmacokinetics (e.g. preload) [7].

To be clinically applied, the developed algorithm requires an individualised PBPK model (i.e. a virtual patient). Individualisation of the  $^{177}\text{Lu}$ -DOTATATE PBPK model for the first cycle can be achieved with at least one data point of a quantitative pretherapeutic imaging modality (e.g. SPECT or PET) [16]. For subsequent  $^{177}\text{Lu}$ -DOTATATE cycles, images from a previous cycle can be used to individualise the model as there may be inter-cycle changes (e.g. in tumour size). If quantitative images are not available, different levels of individualisation can be applied to the PBPK model for treatment planning (the more individualised, the better) [16].

Lastly, the short simulation time ( $< 3$  min for 51 peptide amounts) allows feasible implementation of the developed treatment planning algorithm in clinical routine.

## 6 CONCLUSIONS

The results of the conducted *in silico* clinical trial indicate that the developed treatment planning algorithm can derive plans which produce a higher tumour control than the *typically* delivered plan within tolerated BED constraints for the OARs and considering limitations of the radiopharmaceutical synthesis. The results show that the *typical* plan may be insufficient to produce adequate tumour control after a 4-cycle treatment with  $^{177}\text{Lu}$ -DOTATATE. In contrast, it was shown that the optimal plans derived with the developed treatment planning algorithm may produce adequate tumour control in most patients after 4 cycles of  $^{177}\text{Lu}$ -DOTATATE. This demonstrates the importance of individualised treatment planning in molecular radiotherapy.

The simulated results confirm that both the kidneys and the red marrow need to be included in the treatment planning process for PRRT with  $^{177}\text{Lu}$ -DOTATATE. In addition, higher molar activities than those routinely used for  $^{177}\text{Lu}$ -DOTATATE may be required to achieve better therapeutic outcomes. Furthermore, the short computational time required to complete the individual optimisation process allows the developed algorithm to be feasibly implemented in clinical routine.

Therefore, based on the expected advantages of the developed treatment planning algorithm, this algorithm is proposed for clinical validation and potential future implementation in treatment planning in molecular radiotherapy.

## 7 SUMMARY

Peptide-receptor radionuclide therapy (PRRT) is a modality of molecular radiotherapy in which patients are administered with radiolabelled peptides targeting peptide-receptors overexpressed in some types of tumours. PRRT has shown promising results in the treatment of tumours with high expression of somatostatin receptors (e.g. neuroendocrine tumours (NETs) and meningioma). However, this therapeutic modality potentially produces high radiotoxicity in the kidneys and in the red bone marrow (RM), the kidneys usually being the dose-limiting organ in PRRT. To safely applied PRRT to patients producing an increased therapeutic effect, individualised treatment planning is required. Recently, it was shown that individually choosing an optimal combination of radiopharmaceutical amount and activity may lead to higher therapeutic indices (i.e. the ratio between the tumour dose and the dose in the dose-limiting organ). However, some additional features are required during treatment planning to achieve a clinical applicability in PRRT:

1. Multiple tumour lesions/metastases need to be considered simultaneously.
2. Multiple potentially dose-limiting organs need to be included.
3. Constraints in the radiopharmaceutical synthesis need to be accounted for.

Therefore, the aim of this work was to develop a treatment planning algorithm for PRRT which can be applied clinically. Additionally, an *in silico* (i.e. based on computational simulations) clinical trial was conducted to demonstrate the applicability and advantages of the developed algorithm.

To allow the developed algorithm to be applied for patients with multiple metastases the concept of overall biologically effective dose (oBED) was developed. oBED is a biologically effective dose (BED) value computed considering the total number of killed cells after radiotherapy and that can be used to represent organs/tissues with inhomogeneous characteristics or distribution (e.g. multiple tumour lesions). Therefore, maximising the tumour oBED during treatment planning will derive plans producing the maximum number of killed tumour cells among selected tumour lesions. In addition, the developed treatment planning algorithm incorporates multiple potentially dose-limiting organs and considers the maximum molar activity (i.e. the ratio between activity and amount) which can be achieved during the radiopharmaceutical synthesis. Thus, the developed treatment plan algorithm derives PRRT plans which maximise the total number of tumour cells within tolerated dose values for multiple organs at risk (OARs) and that considers the maximum achievable molar activity in the radiopharmaceutical synthesis.

An *in silico* clinical trial was conducted with nine virtual patients created by fitting a physiologically-based pharmacokinetic (PBPK) model to  $^{111}\text{In}$ -DOTATATE pharmacokinetic data from nine patients with NETs or meningioma. The virtual patients were subsequently adapted to  $^{177}\text{Lu}$ -DOTATATE by changing the nuclide half-life in the virtual patients. In this trial, plans individually derived with the

developed algorithm were compared with the routinely delivered plan for  $^{177}\text{Lu}$ -DOTATATE. Comparison between the optimal plans and the *typical* plan was drawn considering the tumour BED and the overall tumour control probability (oTCP). Complete plans (i.e. after 4 cycles of  $^{177}\text{Lu}$ -DOTATATE) leading to oTCP values higher than 99% were considered as plan producing adequate tumour control.

The results of the conducted *in silico* clinical trial show that the plans derived with the developed algorithm produce considerably higher tumour BED values than the *typical* plan. In addition, the plans derived with the developed algorithm produced adequate tumour control in most (6 out of 9) virtual patients while the *typical* plan produced adequate tumour control in only 2 virtual patients. Therefore, based on the expected advantages, the developed algorithm is proposed for clinical validation and potential clinical implementation.

## 8 REFERENCES

- [1] Seystahl K, Stoecklein V, Schüller U, Rushing E, Nicolas G, Schafer N, et al. Somatostatin receptor-targeted radionuclide therapy for progressive meningioma: benefit linked to  $^{68}\text{Ga}$ -DOTATATE/-TOC uptake. *Neuro Oncol*. 2016;18:1538-47.
- [2] Kreissl MC, Hänscheid H, Löhr M, Verburg FA, Schiller M, Lassmann M, et al. Combination of peptide receptor radionuclide therapy with fractionated external beam radiotherapy for treatment of advanced symptomatic meningioma. *Radiat Oncol*. 2012;7:99.
- [3] Bodei L, Mueller-Brand J, Baum RP, Pavel ME, Horsch D, O'Dorisio MS, et al. The joint IAEA, EANM, and SNMMI practical guidance on peptide receptor radionuclide therapy (PRRNT) in neuroendocrine tumours. *Eur J Nucl Med Mol Imaging*. 2013;40:800-16.
- [4] Kletting P, Kull T, Maaß C, Malik N, Luster M, Beer AJ, et al. Optimized Peptide Amount and Activity for  $^{90}\text{Y}$ -Labeled DOTATATE Therapy. *J Nucl Med*. 2016;57:503-8.
- [5] Dash A, Chakraborty S, Pillai MR, Knapp Jr. FF. Peptide receptor radionuclide therapy: an overview. *Cancer Biother Radiopharm*. 2015;30:47-71.
- [6] Cremonesi M, Ferrari M, Di Dia A, Botta F, De Cicco C, Bodei L, et al. Recent issues on dosimetry and radiobiology for peptide receptor radionuclide therapy. *Q J Nucl Med Mol Imaging*. 2011;55:155-67.
- [7] Glatting G, Bardiès M, Lassmann M. Treatment planning in molecular radiotherapy. *Z Med Phys*. 2013;23:262-9.
- [8] Larson SM, Carrasquillo JA, Cheung NK, Press OW. Radioimmunotherapy of human tumours. *Nat Rev Cancer*. 2015;15:347-60.
- [9] Sharkey RM, Goldenberg DM. Cancer radioimmunotherapy. *Immunotherapy*. 2011;3:349-70.
- [10] Lee SL. Radioactive iodine therapy. *Curr Opin Endocrinol Diabetes Obes*. 2012;19:420-8.
- [11] Sgouros G. Update: molecular radiotherapy: survey and current status. *Cancer Biother Radiopharm*. 2008;23:531-40.
- [12] Gudkov SV, Shilyagina NY, Vodeneev VA, Zvyagin AV. Targeted Radionuclide Therapy of Human Tumors. *Int J Mol Sci*. 2015;17.
- [13] Dash A, Chakraborty S, Pillai MR, Knapp FF, Jr. Peptide receptor radionuclide therapy: an overview. *Cancer Biother Radiopharm*. 2015;30:47-71.
- [14] Cremonesi M, Botta F, Di Dia A, Ferrari M, Bodei L, De Cicco C, et al. Dosimetry for treatment with radiolabelled somatostatin analogues. A review. *Q J Nucl Med Mol Imaging*. 2010;54:37-51.
- [15] Lakshmanan A, Scarberry D, Shen DH, Jhiang SM. Modulation of Sodium Iodide Symporter in Thyroid Cancer. *Horm Cancer-Us*. 2014;5:363-73.
- [16] Hardiansyah D, Maass C, Attarwala AA, Muller B, Kletting P, Mottaghy FM, et al. The role of patient-based treatment planning in peptide receptor radionuclide therapy. *Eur J Nucl Med Mol Imaging*. 2016;43:871-80.



- [17] Kletting P, Kull T, Bunjes D, Mahren B, Luster M, Reske SN, et al. Radioimmunotherapy with anti-CD66 antibody: improving the biodistribution using a physiologically based pharmacokinetic model. *J Nucl Med*. 2010;51:484-91.
- [18] Kletting P, Maaß C, Reske S, Beer AJ, Glatting G. Physiologically Based Pharmacokinetic Modeling Is Essential in  $^{90}\text{Y}$ -Labeled Anti-CD66 Radioimmunotherapy. *PLoS One*. 2015;10:e0127934.
- [19] Kletting P, Schuchardt C, Kulkarni HR, Shahinfar M, Singh A, Glatting G, et al. Investigating the Effect of Ligand Amount and Injected Therapeutic Activity: A Simulation Study for  $^{177}\text{Lu}$ -Labeled PSMA-Targeting Peptides. *PLoS One*. 2016;11:e0162303.
- [20] Jamous M, Haberkorn U, Mier W. Synthesis of peptide radiopharmaceuticals for the therapy and diagnosis of tumor diseases. *Molecules*. 2013;18:3379-409.
- [21] Liu G, Hnatowich DJ. Labeling biomolecules with rhenium: a review of the bifunctional chelators. *Anticancer Agents Med Chem*. 2007;7:367-77.
- [22] Morgan WF, Sowa MB. Non-targeted effects induced by ionizing radiation: mechanisms and potential impact on radiation induced health effects. *Cancer Lett*. 2015;356:17-21.
- [23] Rosch F, Herzog H, Qaim SM. The Beginning and Development of the Theranostic Approach in Nuclear Medicine, as Exemplified by the Radionuclide Pair (86)Y and (90)Y. *Pharmaceuticals (Basel)*. 2017;10.
- [24] Sugiura G, Kuhn H, Sauter M, Haberkorn U, Mier W. Radiolabeling strategies for tumor-targeting proteinaceous drugs. *Molecules*. 2014;19:2135-65.
- [25] Breeman WA, Chan HS, de Zanger RM, Konijnenberg MK, de Blois E. Overview of Development and Formulation of  $^{177}\text{Lu}$ -DOTA-TATE for PRRT. *Curr Radiopharm*. 2016;9:8-18.
- [26] Coenen HH, Gee AD, Adam M, Antoni G, Cutler CS, Fujibayashi Y, et al. Open letter to journal editors on: International Consensus Radiochemistry Nomenclature Guidelines. *Ann Nucl Med*. 2018.
- [27] Baldari S, Ferrau F, Alafaci C, Herberg A, Granata F, Militano V, et al. First demonstration of the effectiveness of peptide receptor radionuclide therapy (PRRT) with  $^{111}\text{In}$ -DTPA-octreotide in a giant PRL-secreting pituitary adenoma resistant to conventional treatment. *Pituitary*. 2012;15 Suppl 1:S57-60.
- [28] Dong C, Liu Z, Wang F. Peptide-based radiopharmaceuticals for targeted tumor therapy. *Curr Med Chem*. 2014;21:139-52.
- [29] Reynolds TS, Bandari RP, Jiang Z, Smith CJ. Lutetium-177 Labeled Bombesin Peptides for Radionuclide Therapy. *Curr Radiopharm*. 2016;9:33-43.
- [30] Krzan M, Vianello R, Marsavelski A, Repic M, Zaksek M, Kotnik K, et al. The Quantum Nature of Drug-Receptor Interactions: Deuteration Changes Binding Affinities for Histamine Receptor Ligands. *PLoS One*. 2016;11:e0154002.
- [31] Alix K, Khatri S, Mosier PD, Casterlow S, Yan D, Nyce HL, et al. Superagonist, Full Agonist, Partial Agonist, and Antagonist Actions of Arylguanidines at 5-Hydroxytryptamine-3 (5-HT<sub>3</sub>) Subunit A Receptors. *ACS Chem Neurosci*. 2016;7:1565-74.

- [32] Yang J, Chang CY, Safi R, Morgan J, McDonnell DP, Fuller PJ, et al. Identification of ligand-selective peptide antagonists of the mineralocorticoid receptor using phage display. *Mol Endocrinol*. 2011;25:32-43.
- [33] Fani M, Nicolas GP, Wild D. Somatostatin Receptor Antagonists for Imaging and Therapy. *J Nucl Med*. 2017;58:61S-6S.
- [34] Ljungberg M, Sjögreen Gleisner K. Personalized Dosimetry for Radionuclide Therapy Using Molecular Imaging Tools. *Biomedicines*. 2016;4.
- [35] Rolleman EJ, Valkema R, de Jong M, Kooij PP, Krenning EP. Safe and effective inhibition of renal uptake of radiolabelled octreotide by a combination of lysine and arginine. *Eur J Nucl Med Mol Imaging*. 2003;30:9-15.
- [36] Kraeber-Bodere F, Barbet J, Chatal JF. Radioimmunotherapy: From Current Clinical Success to Future Industrial Breakthrough? *J Nucl Med*. 2016;57:329-31.
- [37] Fan J, de Lannoy IA. Pharmacokinetics. *Biochem Pharmacol*. 2014;87:93-120.
- [38] Lipman NS, Jackson LR, Trudel LJ, Weis-Garcia F. Monoclonal versus polyclonal antibodies: distinguishing characteristics, applications, and information resources. *ILAR J*. 2005;46:258-68.
- [39] Weiner GJ. Building better monoclonal antibody-based therapeutics. *Nat Rev Cancer*. 2015;15:361-70.
- [40] Evans HL, Nguyen QD, Carroll LS, Kaliszczak M, Twyman FJ, Spivey AC, et al. A bioorthogonal (68)Ga-labelling strategy for rapid in vivo imaging. *Chem Commun (Camb)*. 2014;50:9557-60.
- [41] Urso R, Blardi P, Giorgi G. A short introduction to pharmacokinetics. *Eur Rev Med Pharmacol Sci*. 2002;6:33-44.
- [42] Koch-Weser J, Sellers EM. Binding of drugs to serum albumin (first of two parts). *N Engl J Med*. 1976;294:311-6.
- [43] Bolch WE, Eckerman KF, Sgouros G, Thomas SR. MIRD pamphlet No. 21: a generalized schema for radiopharmaceutical dosimetry--standardization of nomenclature. *J Nucl Med*. 2009;50:477-84.
- [44] Stabin MG, Sparks RB, Crowe E. OLINDA/EXM: the second-generation personal computer software for internal dose assessment in nuclear medicine. *J Nucl Med*. 2005;46:1023-7.
- [45] Hindorf C, Glatting G, Chiesa C, Lindén O, Flux G, Committee ED. EANM Dosimetry Committee guidelines for bone marrow and whole-body dosimetry. *Eur J Nucl Med Mol Imaging*. 2010;37:1238-50.
- [46] Glatting G, Kletting P, Reske SN, Hohl K, Ring C. Choosing the optimal fit function: comparison of the Akaike information criterion and the F-test. *Med Phys*. 2007;34:4285-92.
- [47] Aarons L. Physiologically based pharmacokinetic modelling: a sound mechanistic basis is needed. *Br J Clin Pharmacol*. 2005;60:581-3.

- [48] Hu X, Olivier K, Polack E, Crossman M, Zokowski K, Gronke RS, et al. In vivo pharmacology and toxicology evaluation of polyethylene glycol-conjugated interferon beta-1a. *J Pharmacol Exp Ther*. 2011;338:984-96.
- [49] Lindstedt SL, Schaeffer PJ. Use of allometry in predicting anatomical and physiological parameters of mammals. *Lab Anim*. 2002;36:1-19.
- [50] Barrett PH, Bell BM, Cobelli C, Golde H, Schumitzky A, Vicini P, et al. SAAM II: Simulation, Analysis, and Modeling Software for tracer and pharmacokinetic studies. *Metabolism*. 1998;47:484-92.
- [51] Krauss M, Tappe K, Schuppert A, Kuepfer L, Goerlitz L. Bayesian Population Physiologically-Based Pharmacokinetic (PBPK) Approach for a Physiologically Realistic Characterization of Interindividual Variability in Clinically Relevant Populations. *PLoS One*. 2015;10:e0139423.
- [52] Vizirianakis IS, Mystridis GA, Avgoustakis K, Fatouros DG, Spanakis M. Enabling personalized cancer medicine decisions: The challenging pharmacological approach of PBPK models for nanomedicine and pharmacogenomics (Review). *Oncol Rep*. 2016;35:1891-904.
- [53] Grudzinski JJ, Tomé W, Weichert JP, Jeraj R. The biological effectiveness of targeted radionuclide therapy based on a whole-body pharmacokinetic model. *Phys Med Biol*. 2010;55:5723-34.
- [54] Lassmann M, Chiesa C, Flux G, Bardies M, Committee ED. EANM Dosimetry Committee guidance document: good practice of clinical dosimetry reporting. *Eur J Nucl Med Mol Imaging*. 2011;38:192-200.
- [55] Howell RW, Wessels BW, Loevinger R, Watson EE, Bolch WE, Brill AB, et al. The MIRD perspective 1999. Medical Internal Radiation Dose Committee. *J Nucl Med*. 1999;40:3S-10S.
- [56] Stabin MG, Siegel JA. RADAR Dose Estimate Report: A Compendium of Radiopharmaceutical Dose Estimates Based on OLINDA/EXM Version 2.0. *J Nucl Med*. 2018;59:154-60.
- [57] Reisz JA, Bansal N, Qian J, Zhao W, Furdui CM. Effects of ionizing radiation on biological molecules--mechanisms of damage and emerging methods of detection. *Antioxid Redox Signal*. 2014;21:260-92.
- [58] Higo T, Naito AT, Sumida T, Shibamoto M, Okada K, Nomura S, et al. DNA single-strand break-induced DNA damage response causes heart failure. *Nat Commun*. 2017;8:15104.
- [59] Caldecott KW. Single-strand break repair and genetic disease. *Nat Rev Genet*. 2008;9:619-31.
- [60] Brenner DJ. The linear-quadratic model is an appropriate methodology for determining isoeffective doses at large doses per fraction. *Semin Radiat Oncol*. 2008;18:234-9.
- [61] Kehwar TS, Chopra KL, Rai DV. A Unified Dose Response Relationship to Predict High Dose Fractionation Response in the Lung Cancer Stereotactic Body Radiation Therapy. *J Med Phys*. 2017;42:222-33.
- [62] Stokke C, Gabina PM, Solny P, Cicone F, Sandstrom M, Gleisner KS, et al. Dosimetry-based treatment planning for molecular radiotherapy: a summary of the 2017 report from the Internal Dosimetry Task Force. *EJNMMI Phys*. 2017;4:27.

- [63] Kletting P, Meyer C, Reske SN, Glatting G. Potential of optimal preloading in anti-CD20 antibody radioimmunotherapy: an investigation based on pharmacokinetic modeling. *Cancer Biother Radiopharm.* 2010;25:279-87.
- [64] Kletting P, Kull T, Bunjes D, Luster M, Reske SN, Glatting G. Optimal preloading in radioimmunotherapy with anti-cD45 antibody. *Med Phys.* 2011;38:2572-8.
- [65] Sundlov A, Sjögreen-Gleisner K, Svensson J, Ljungberg M, Olsson T, Bernhardt P, et al. Individualised  $^{177}\text{Lu}$ -DOTATATE treatment of neuroendocrine tumours based on kidney dosimetry. *Eur J Nucl Med Mol Imaging.* 2017;44:1480-9.
- [66] Jiménez-Franco LD, Kletting P, Beer AJ, Glatting G. Treatment planning algorithm for PRRT considering multiple tumor lesions and organs at risk. *Med Phys.* 2018:(in revision datum).
- [67] Sachs RK, Hlatky LR. Dose-rate dependent stochastic effects in radiation cell-survival models. *Radiat Environ Biophys.* 1990;29:169-84.
- [68] Konijnenberg MW, Breeman WA, de Blois E, Chan HS, Boerman OC, Laverman P, et al. Therapeutic application of CCK2R-targeting PP-F11: influence of particle range, activity and peptide amount. *EJNMMI Res.* 2014;4:47.
- [69] Hillen T, de Vries G, Gong J, Finlay C. From cell population models to tumor control probability: including cell cycle effects. *Acta Oncol.* 2010;49:1315-23.
- [70] de Laat JM, Pieterman CR, van den Broek MF, Twisk JW, Hermus AR, Dekkers OM, et al. Natural course and survival of neuroendocrine tumors of thymus and lung in MEN1 patients. *J Clin Endocrinol Metab.* 2014;99:3325-33.
- [71] Evers S, Verbaan D, Sanchez E, Peerdeman S. 3D Volumetric Measurement of Neurofibromatosis Type 2-Associated Meningiomas: Association Between Tumor Location and Growth Rate. *World Neurosurg.* 2015;84:1062-9.
- [72] Bergsma H, Konijnenberg MW, van der Zwan WA, Kam BL, Teunissen JJ, Kooij PP, et al. Nephrotoxicity after PRRT with  $^{177}\text{Lu}$ -DOTA-octreotate. *Eur J Nucl Med Mol Imaging.* 2016;43:1802-11.
- [73] Zagars GK, Schultheiss TE, Peters LJ. Inter-tumor heterogeneity and radiation dose-control curves. *Radiother Oncol.* 1987;8:353-61.
- [74] Klemenc-Ketis Z, Cagran B, Dinevski D. Evaluating the Difference between Virtual and Paper-Based Clinical Cases in Family Medicine Undergraduate Education. *Advances in Medicine.* 2018;2018:7.
- [75] Chechev VP, Egorov AG. Search for an optimum approach to the evaluation of data of varying consistency: half-live evaluations for  $^3\text{H}$ ,  $^{35}\text{S}$ ,  $^{55}\text{Fe}$ ,  $^{99}\text{Mo}$  and  $^{111}\text{In}$ . *Appl Radiat Isot.* 2000;52:601-8.
- [76] Pommé S, Paepen J, Altizoglou T, Van Ammel R, Yeltepe E. Measurement of the  $^{177}\text{Lu}$  half-life. *Appl Radiat Isot.* 2011;69:1267-73.
- [77] Glatting G, Landmann M, Kull T, Wunderlich A, Blumstein NM, Buck AK, et al. Internal radionuclide therapy: the ULMDOS software for treatment planning. *Med Phys.* 2005;32:2399-405.

- [78] Kletting P, Schimmel S, Hänscheid H, Luster M, Fernandez M, Nosske D, et al. The NUKDOS software for treatment planning in molecular radiotherapy. *Z Med Phys*. 2015;25:264-74.
- [79] Kletting P, Bunjes D, Reske SN, Glatting G. Improving anti-CD45 antibody radioimmunotherapy using a physiologically based pharmacokinetic model. *J Nucl Med*. 2009;50:296-302.
- [80] Delpassand ES, Samarghandi A, Zamanian S, Wolin EM, Hamiditabar M, Espenan GD, et al. Peptide receptor radionuclide therapy with  $^{177}\text{Lu}$ -DOTATATE for patients with somatostatin receptor-expressing neuroendocrine tumors: the first US phase 2 experience. *Pancreas*. 2014;43:518-25.
- [81] Myler HR. Fundamentals of engineering programming with C and Fortran. Cambridge; New York: Cambridge University Press; 1998.
- [82] Hamiditabar M, Ali M, Roys J, Wolin EM, O'Dorisio TM, Ranganathan D, et al. Peptide Receptor Radionuclide Therapy With  $^{177}\text{Lu}$ -Octreotate in Patients With Somatostatin Receptor Expressing Neuroendocrine Tumors: Six Years' Assessment. *Clin Nucl Med*. 2017;42:436-43.
- [83] Bodei L, Cremonesi M, Ferrari M, Pacifici M, Grana CM, Bartolomei M, et al. Long-term evaluation of renal toxicity after peptide receptor radionuclide therapy with  $^{90}\text{Y}$ -DOTATOC and  $^{177}\text{Lu}$ -DOTATATE: the role of associated risk factors. *Eur J Nucl Med Mol Imaging*. 2008;35:1847-56.
- [84] Kwekkeboom DJ, de Herder WW, Kam BL, van Eijck CH, van Essen M, Kooij PP, et al. Treatment with the radiolabeled somatostatin analog [ $^{177}\text{Lu}$ -DOTA $^0$ ,Tyr $^3$ ]octreotate: toxicity, efficacy, and survival. *J Clin Oncol*. 2008;26:2124-30.
- [85] Stabin MG, Siegel JA. Physical models and dose factors for use in internal dose assessment. *Health Phys*. 2003;85:294-310.
- [86] Fowler JF. 21 years of biologically effective dose. *Br J Radiol*. 2010;83:554-68.
- [87] Cremonesi M, Chiesa C, Strigari L, Ferrari M, Botta F, Guerriero F, et al. Radioembolization of hepatic lesions from a radiobiology and dosimetric perspective. *Front Oncol*. 2014;4:210.
- [88] Konijnenberg M. From imaging to dosimetry and biological effects. *Q J Nucl Med Mol Imaging*. 2011;55:44-56.
- [89] Dale RG. The application of the linear-quadratic dose-effect equation to fractionated and protracted radiotherapy. *Br J Radiol*. 1985;58:515-28.
- [90] Kwekkeboom DJ, Bakker WH, Kooij PP, Konijnenberg MW, Srinivasan A, Erion JL, et al. [ $^{177}\text{Lu}$ -DOTA $^0$ ,Tyr $^3$ ]octreotate: comparison with [ $^{111}\text{In}$ -DTPA $^0$ ]octreotide in patients. *Eur J Nucl Med*. 2001;28:1319-25.
- [91] Baker F, Sanger L. The density of clonogenic cells in human solid tumors. *Int J Cell Cloning*. 1991;9:155-65.
- [92] O'Donoghue JA. Implications of nonuniform tumor doses for radioimmunotherapy. *J Nucl Med*. 1999;40:1337-41.

- [93] Cremonesi M, Ferrari M, Botta F, Guerriero F, Garibaldi C, Bodei L, et al. Planning combined treatments of external beam radiation therapy and molecular radiotherapy. *Cancer Biother Radiopharm.* 2014;29:227-37.
- [94] Kauwelo K, Papanikolaou N, Stathakis S, Esquivel C, Crownover R, Mavroidis P. SU-E-T-714: Analysis of Two Overall Biological Effective Dose (OBED) Calculation Methods and Their Impact On the Accurate Determination of the Maximum Biological Effective Dose (BED) in Multi-Phase Treatment Plans. *Medical Physics.* 2013;40:370-.
- [95] Kletting P, Thieme A, Eberhardt N, Rinscheid A, D'Alessandria C, Allmann J, et al. Modeling and predicting tumor response in radioligand therapy. *J Nucl Med.* 2018.
- [96] Webb S, Nahum AE. A model for calculating tumour control probability in radiotherapy including the effects of inhomogeneous distributions of dose and clonogenic cell density. *Phys Med Biol.* 1993;38:653-66.
- [97] Nahum AE, Uzan J. (Radio)biological optimization of external-beam radiotherapy. *Comput Math Methods Med.* 2012;2012:329214.
- [98] Niemierko A, Goitein M. Implementation of a model for estimating tumor control probability for an inhomogeneously irradiated tumor. *Radiother Oncol.* 1993;29:140-7.
- [99] Wiklund K, Toma-Dasu I, Lind BK. Impact of dose and sensitivity heterogeneity on TCP. *Comput Math Methods Med.* 2014;2014:182935.
- [100] Sandström M, Garske-Roman U, Johansson S, Granberg D, Sundin A, Freedman N. Kidney dosimetry during <sup>177</sup>Lu-DOTATATE therapy in patients with neuroendocrine tumors: aspects on calculation and tolerance. *Acta Oncol.* 2018;57:516-21.
- [101] Sandström M, Garske-Roman U, Granberg D, Johansson S, Widstrom C, Eriksson B, et al. Individualized dosimetry of kidney and bone marrow in patients undergoing <sup>177</sup>Lu-DOTA-octreotate treatment. *J Nucl Med.* 2013;54:33-41.
- [102] Sundlöv A, Sjögren-Gleisner K, Svensson J, Ljungberg M, Olsson T, Bernhardt P, et al. Individualised <sup>177</sup>Lu-DOTATATE treatment of neuroendocrine tumours based on kidney dosimetry. *Eur J Nucl Med Mol Imaging.* 2017;44:1480-9.
- [103] Bison SM, Pool SE, Koelewijn SJ, van der Graaf LM, Groen HC, Melis M, et al. Peptide receptor radionuclide therapy (PRRT) with [(177)Lu-DOTA(0),Tyr(3)]octreotate in combination with RAD001 treatment: further investigations on tumor metastasis and response in the rat pancreatic CA20948 tumor model. *EJNMMI Res.* 2014;4:21.
- [104] Kunikowska J, Krolicki L, Hubalewska-Dydejczyk A, Mikolajczak R, Sowa-Staszczak A, Pawlak D. Clinical results of radionuclide therapy of neuroendocrine tumours with 90Y-DOTATATE and tandem 90Y/177Lu-DOTATATE: which is a better therapy option? *Eur J Nucl Med Mol Imaging.* 2011;38:1788-97.
- [105] Begum N, Thieme A, Eberhardt N, Tauber R, Beer AJ, Glatting G, et al. The effect of total tumor volume on the biologically effective dose of tumor and kidneys for <sup>177</sup>Lu-labelled PSMA peptides. *J Nucl Med.* 2018. epub 01.02.18.

## APPENDIX A: ABSORBED DOSE CALCULATIONS

In this work, because of the short penetration depth of  $^{177}\text{Lu}$  (1.7 mm), only radiation produced in each respective organ/lesion (i.e.  $S_{(rT \leftarrow rS)} = 0$  for  $rT \neq rS$  in Eq. (6)) was considered for absorbed dose calculations in the tumour lesions, kidneys, liver and spleen. For the RM, as it is a distributed organ with high radiosensitivity, radiation produced in every organ included in the PBPK model was considered.

Dose factors for  $^{177}\text{Lu}$  for the OARs were extracted from OLINDA/EXM [44] and scaled based on the size of the target organ. The scaling factor ( $k_{rT}$ ) for the dose factors was defined as:

$$k_{rT} = \frac{m_{rT\_patient}}{m_{rT\_phantom}} \quad (\text{A1})$$

where  $m_{rT\_patient}$  is the mass of the target organ in the patient (measured or scaled) and  $m_{rT\_phantom}$  is the mass of the target organ used in OLINDA/EXM [44]. Dose factors for the RM were scaled based on patient body weight (Table II). Dose factors for  $^{177}\text{Lu}$  extracted from OLINDA/EXM for dose calculations are presented in Table A - I.

**Table A - I.** Dose factors for  $^{177}\text{Lu}$  from OLINDA/EXM [44].

Parameter	Description	Value	Unit
$S_{K \leftarrow K}$	dose factor from kidney to kidney (scaled using organ mass)	$4.82 \times 10^{-6}$	$\text{Gy} \cdot \text{min}^{-1} \cdot \text{MBq}^{-1}$
$S_{L \leftarrow L}$	dose factor from liver to liver (scaled using organ mass)	$7.74 \times 10^{-7}$	$\text{Gy} \cdot \text{min}^{-1} \cdot \text{MBq}^{-1}$
$S_{S \leftarrow S}$	dose factor from spleen to spleen (scaled using organ mass)	$7.86 \times 10^{-6}$	$\text{Gy} \cdot \text{min}^{-1} \cdot \text{MBq}^{-1}$
$S_{RM \leftarrow RM}$	dose factor from red marrow to red marrow (scaled using body weight)	$7.14 \times 10^{-7}$	$\text{Gy} \cdot \text{min}^{-1} \cdot \text{MBq}^{-1}$
$S_{RM \leftarrow REM}$	dose factor from remainder to red marrow (scaled using body weight)	$4.83 \times 10^{-9}{}^a$	$\text{Gy} \cdot \text{min}^{-1} \cdot \text{MBq}^{-1}$
$S_{RM \leftarrow AD}$	dose factor from adrenal glands to red marrow (scaled using body weight)	$4.11 \times 10^{-9}$	$\text{Gy} \cdot \text{min}^{-1} \cdot \text{MBq}^{-1}$
$S_{RM \leftarrow L}$	dose factor from liver to red marrow (scaled using body weight)	$1.39 \times 10^{-9}$	$\text{Gy} \cdot \text{min}^{-1} \cdot \text{MBq}^{-1}$
$S_{RM \leftarrow S}$	dose factor from spleen to red marrow (scaled using body weight)	$1.40 \times 10^{-9}$	$\text{Gy} \cdot \text{min}^{-1} \cdot \text{MBq}^{-1}$
$S_{RM \leftarrow GI}{}^b$	dose factor from gastrointestinal track to red marrow (scaled using body weight)	$2.92 \times 10^{-9}$	$\text{Gy} \cdot \text{min}^{-1} \cdot \text{MBq}^{-1}$
$S_{RM \leftarrow MUS}$	dose factor from muscle to red marrow (scaled using body weight)	$1.52 \times 10^{-9}$	$\text{Gy} \cdot \text{min}^{-1} \cdot \text{MBq}^{-1}$
$S_{RM \leftarrow LU}$	dose factor from lungs to red marrow (scaled using body weight)	$1.84 \times 10^{-9}$	$\text{Gy} \cdot \text{min}^{-1} \cdot \text{MBq}^{-1}$
$S_{RM \leftarrow K}$	dose factor from kidneys to red marrow (scaled using body weight)	$2.84 \times 10^{-9}$	$\text{Gy} \cdot \text{min}^{-1} \cdot \text{MBq}^{-1}$
$S_{RM \leftarrow BR}$	dose factor from brain to red marrow (scaled using body weight)	$1.65 \times 10^{-9}$	$\text{Gy} \cdot \text{min}^{-1} \cdot \text{MBq}^{-1}$
$S_{RM \leftarrow HRT}$	dose factor from heart to red marrow (scaled using body weight)	$1.82 \times 10^{-9}$	$\text{Gy} \cdot \text{min}^{-1} \cdot \text{MBq}^{-1}$
$S_{RM \leftarrow RM}{}^c$	dose factor from bone to red marrow (scaled using body weight)	$2.04 \times 10^{-7}$	$\text{Gy} \cdot \text{min}^{-1} \cdot \text{MBq}^{-1}$
$S_{WB \leftarrow WB}$	dose factor from whole body to whole body (scaled using body weight)	$2.14 \times 10^{-8}$	$\text{Gy} \cdot \text{min}^{-1} \cdot \text{MBq}^{-1}$

<sup>a</sup> Value calculated based on Hindorf et al. [45] with data from OLINDA/EXM [44].

<sup>b</sup> Dose factor for the for the small intestine.

<sup>c</sup> Dose factor for trabecular bone.

Dose factors for  $^{177}\text{Lu}$  for the tumour lesions were fitted to published data [85] based on the tumour lesion mass. A tumour density of 1 g/ml was assumed. The data used for this fitting are presented in Table A - II.



**Table A - II.** Reported dose factors for  $^{177}\text{Lu}$  for tumour lesions based on tumour mass [85].

Tumour mass [g]	Tumour dose factor [Gy·min <sup>-1</sup> ·MBq <sup>-1</sup> ]
0.5	$2.77 \times 10^{-3}$
1	$1.40 \times 10^{-3}$
1.5	$9.00 \times 10^{-4}$
2	$7.02 \times 10^{-4}$
3	$4.50 \times 10^{-4}$
4	$3.52 \times 10^{-4}$
13	$1.10 \times 10^{-4}$
17	$8.30 \times 10^{-5}$
21	$6.90 \times 10^{-5}$
29	$4.80 \times 10^{-5}$
34	$4.30 \times 10^{-5}$
52	$2.67 \times 10^{-5}$
54	$2.65 \times 10^{-5}$

The fitted function for the tumour dose factors used for the dose calculations is:

$$S_{TU} = 1.407 \cdot 10^{-3} \cdot m_{TU}^{-1} - 3.724 \cdot 10^{-5} \cdot m_{TU}^{(-2/3)} + 1.403 \cdot 10^{-5} \cdot m_{TU}^{(-1/3)} \quad (\text{A2})$$

where  $S_{TU}$  is the dose factor for a tumour lesion [Gy·min<sup>-1</sup>·MBq<sup>-1</sup>] and  $m_{TU}$  is the mass of the tumour lesion [g]. The result of the fitting is presented in Figure A - I.

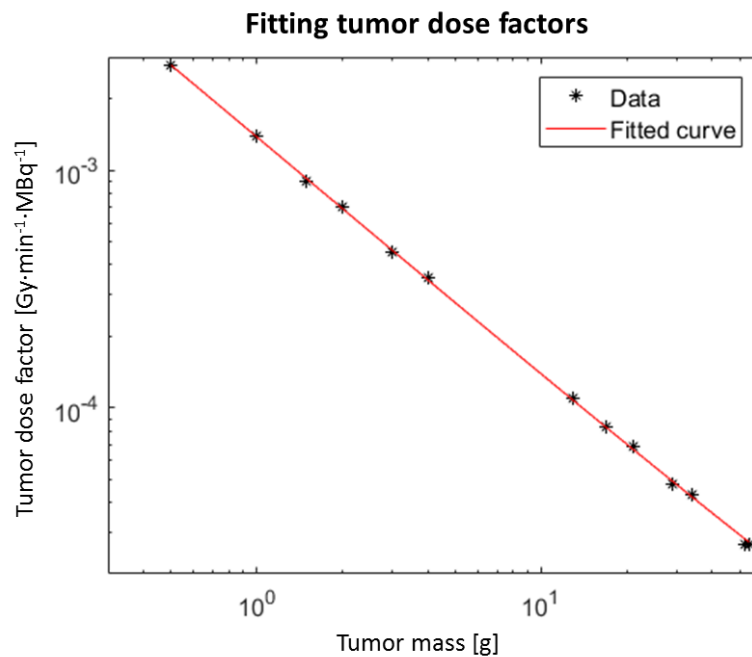


**Figure A - I.** Fit of tumour dose factors for  $^{177}\text{Lu}$ -DOTATATE based on tumour mass. The adjusted  $R^2$  value of the fitting was 0.9998.

## APPENDIX B: LIVER AND SPLEEN RESULTS

Dose calculations for the liver and spleen for the optimal plans and for the *typically* delivered plan are presented in Table A - III. In this table, the molar activities for the optimal plans derived by using the developed treatment planning algorithm are also presented.

**Table A - III.** Molar activities (MA) for the optimal plans and BEDs and absorbed doses (D) for the liver and spleen for the optimal plan and *typically* delivered plans. Results corresponding to simulations of the first cycle of  $^{177}\text{Lu}$ -DOTATATE PRRT for nine virtual patients.

Virtual Patient (Tumour)	Optimal Plan			<i>Typically</i> delivered plan <sup>a</sup>	
	MA [MBq/nmol]	BED <sub>L</sub> [Gy <sub>2.5</sub> ] (D <sub>L</sub> [Gy])	BED <sub>S</sub> [Gy <sub>2.5</sub> ] (D <sub>S</sub> [Gy])	BED <sub>L</sub> [Gy <sub>2.5</sub> ] (D <sub>L</sub> [Gy])	BED <sub>S</sub> [Gy <sub>2.5</sub> ] (D <sub>S</sub> [Gy])
VP1 (M)	139	2.2 (2.2)	14.5 (12.5)	0.75 (0.75)	4.3 (4.1)
VP2 (M)	125	1.8 (1.7)	15.0 (13.0)	0.58 (0.58)	4.3 (4.1)
VP3 (M)	58	1.3 (1.3)	25.9 (21.0)	0.47 (0.47)	9.3 (8.5)
VP4 (M)	205	1.2 (1.2)	16.0 (12.5)	0.37 (0.37)	3.7 (3.4)
VP5 (N)	122	1.0 (1.0)	11.9 (9.67)	0.64 (0.63)	6.1 (5.5)
VP6 (N) <sup>b</sup>	257	1.6 (1.6)	-	0.52 (0.51)	-
VP7 (N)	223	3.8 (3.6)	14.5 (12.1)	0.81 (0.80)	2.7 (2.6)
VP8 (N)	143	2.1 (2.1)	18.1 (15.3)	0.78 (0.78)	5.3 (5.0)
VP9 (N)	73	2.4 (2.3)	23.6 (17.7)	1.4 (1.3)	11.8 (10.0)
Median	139	1.8 (1.7)	15.5 (12.8)	0.64 (0.63)	4.8 (4.6)
Min.	58	1.0 (1.0)	11.9 (9.7)	0.37 (0.37)	2.7 (2.6)
Max.	257	3.8 (3.6)	25.9 (21.0)	1.4 (1.3)	11.8 (10.0)

<sup>a</sup> Molar activity for the *typically* delivered plan = 28 MBq/nmol.

<sup>b</sup> Splenectomy.

MA, molar activity; M, meningioma; N, neuroendocrine tumour; D, absorbed dose.

Subscripts L and S stand for liver and spleen, respectively.

# CURRICULUM VITAE

## Personal Information

First name	Luis David
Family name	Jiménez Franco
Date of birth	03 June, 1983
Place of birth	Medellín, Colombia
Nationality	Colombian
Marital status	Single

## Education

Jan/16 – Present	PhD student in Medical Physics Medical Faculty Mannheim Heidelberg University, Heidelberg – Germany
Sep/14 – Aug/15	Master of Science in Medical Physics Heidelberg University, Heidelberg – Germany <u>Cumulative Master Grade: 1.4 (Sehr Gut)</u>
Feb/11 – Jun/13	Master of Science in Engineering Universidad EAFIT, Medellín - Colombia <u>Cumulative Master Grade: GPA of 4.57/5.0</u>
Jan /01 – Feb/09	Bachelor in Electronic Engineering Universidad Pontificia Bolivariana, Medellín - Colombia <u>Cumulative Bachelor Grade: GPA of 4.39/5.0</u>
Jan/89 – Dec/00	High School Graduation Colegio Corazonista, Medellín – Colombia

## Professional Experience

Sep/15 – Present	Trainee in Medical Physics University Medical Centre Mannheim – Germany
Jul/12 – Nov/13	Undergraduate Lecturer Department of Design Engineering Universidad EAFIT, Medellín - Colombia
Sep/09 – Feb/12	Electronic Development Engineer C.I. TIG - Technology in bathroom fittings, Medellín – Colombia
Jul/05 – Jun/07	Maintenance Engineer Renault - SOFASA, Medellín – Colombia

## PUBLICATIONS

### Original Article

1. **Jiménez-Franco LD**, Kletting P, Beer AJ, Glatting G. Treatment planning algorithm for PRRT considering multiple tumour lesions and organs at risk. Med Phys 2018; (in revision datum).

### Conference Presentations

1. **L. D. Jimenez**, A. K. Leszczynska, G. Glatting. Allometric scaling of organ volumes and blood flows to generate Bayes parameters for use in PBPK models. Nuklearmedizin 2018; 57: A74-75, P51.
2. A. Attarwala, **L. Jimenez**, D. Hardiansyah, P. Kletting, G. Glatting. An algorithm to select the optimal radiopharmaceutical in molecular radiotherapy. Nuklearmedizin 2018; 57: A75, P53.
3. A.A. Asgar, **L.D. Jimenez**, D. Hardiansyah, P. Kletting, G. Glatting. Development of an algorithm for selecting the optimal radiopharmaceutical to molecular radiotherapy. DGMP-DGBMT 2017, Poster session 31: Modelling and simulation IV, P 298.
4. **Jimenez Franco LD**, Kletting P, Glatting G. Treatment planning in PRRT with <sup>177</sup>Lu-DOTATATE considering optimization of the amount, schedule and affinity of a preload substance. J Nucl Med. 2017; 58 (Supplement 1): 131.
5. F. Schneider, **L. D. Jimenez**, F. Bludau, A. Jahnke, C. Illana, J. Fleckenstein, *et al.*, "OC-0362: Precision IORT - image guided IORT including online CBCT based Monte Carlo treatment planning," *Radiotherapy and Oncology*, vol. 123, pp. S194-S195, 2017
6. **Jimenez LD**, Hardiansyah D, Glatting G. Development of a PBPK Model of Arginine Biokinetics in Humans to Optimize Kidney Protection During Peptide Receptor Radionuclide Therapy. Eur J Nucl Med Mol Imaging. 2016; 43 (Supplement 1): S190, OP634.
7. Hardiansyah D, Attarwala AA, **Jimenez LD**, Kletting P, Mottaghy FM, Glatting G. Simulation Study to Determine an Optimal Sampling Schedule for Dynamic PET Measurements for Treatment Planning in Peptide-Receptor Radionuclide Therapy. Eur J Nucl Med Mol Imaging. 2016; 43 (Supplement 1):S120-S121, OP392.

## ACKNOWLEDGEMENTS

First and most importantly, I want to thank God and the Blessed Virgin Mary for the opportunity to conduct this research and for the light to achieve meaningful results. Without God's grace and the intercession of the Virgin Mary this work would not have been possible. The support of my family, especially of my parents, was fundamental to be able to persevere and complete this work. In addition, my parents have always provided me with an environment full of love and opportunities and taught me the importance of responsibility and of a well-done work. This has modelled my character and intellect to be the person and the researcher that I am today. I would also want to express my love, gratitude and admiration to my beautiful Céline, her support, advice and love were fundamental for me to successfully complete my PhD.

Prof. Dr. Gerhard Glatting has taught me almost everything I know about nuclear medicine (I have also read a bit on my own) and helped me very much to develop the concepts and the algorithm presented in this work. Therefore, I am very grateful to him. His best characteristic is that he is able to combine humbleness to consider ideas from others and wisdom and patience to successfully lead those ideas to meaningful results. I would also like to acknowledge Dr. Peter Kletting, whose work inspired me to develop the presented treatment planning algorithm and who provided me with tools required to successfully complete the conducted *in silico* clinical trial. Furthermore, I would like to thank my good friend Dr. Björn Nadrowski, who helped me to develop a fast optimisation algorithm.

To Prof. Dr. med. Frederik Wenz I want to express my total gratitude for his support during my doctoral studies and for presenting this thesis before the Doctoral Committee.

Lastly, I want to gratefully acknowledge funding from the European Union's Seventh Framework Programme under grant agreement No. 602306 (MITIGATE) and from M<sup>2</sup>OLIE (Research Campus funded by the German Federal Ministry of Education and Research (BMBF) within the Framework "Forschungscampus: public-private partnership for Innovations"). I am also grateful to the Medical Faculty Mannheim of the Heidelberg University and the University Medical Centre Mannheim.